Thesis for The Degree of Licentiate of Engineering

Study of MgB_2 HEB mixers at THz frequencies

Evgenii Novoselov

Terahertz and Millimetre Wave Laboratory
Department of Microtechnology and Nanoscience - MC2
Chalmers University of Technology
Göteborg, Sweden 2016

Study of MgB_2 HEB mixers at THz frequencies

EVGENII NOVOSELOV

Chalmers University of Technology
Department of Microtechnology and Nanoscience - MC2
Terahertz and Millimetre Wave Laboratory
SE-412 96 Göteborg, Sweden
Phone: +46 (0) 31 772 1000

ISSN 1652-0769
Technical Report MC2-330

Printed by Chalmers Reproservice
Göteborg, Sweden, 2016

Abstract

The terahertz (THz) range is very attractive for astronomical observations. Spectroscopy and photometry of remote space objects in the THz range allows for a study of their chemical composition, because this range covers rotational lines from simple molecules and electron transition lines from atoms and ions. Heterodyne receivers, due to their high spectral resolution, in the THz range allows for a studying of dynamical behaviour of space objects manifested in doppler-shifted emission lines.

Niobium nitride (NbN) hot-electron bolometer (HEB) mixers currently used at frequencies >1 THz provide a typical gain bandwidth (GBW) of 3–4 GHz which limits the number of astronomical applications. Moreover, the low (8–11 K) critical temperature (T_c) of NbN ultra-thin films necessitates a use of liquid helium (LHe) for the device cooling, which reduce a lifetime of spaceborn missions.

MgB_2 HEB mixers, introduced recently, can solve both of these problems. The high (39 K) T_c and the short (3 ps) electron-phonon interaction time of MgB_2 could provide a bandwidth up to 10 GHz and operation at temperatures >20 K, where compact cryocoolers are available. However, the sensitivity of HEB mixers made from MgB_2 thin films with such a high T_c operating at these temperatures is still in question.

This thesis presents the noise performance study of novel submicron size MgB_2 HEB mixers. Noise temperatures and conversion gains at 1.6 THz local oscillator (LO) of devices with different T_c were investigated with respect to the bath temperature. The minimum Double sideband (DSB) noise temperature for a "low" T_c HEB was 700 K with a 3.2 GHz noise bandwidth (NBW) and 1150 K with a 3.5 GHz NBW for 2.7 K and 4.2 K bath temperatures, respectively. The operation at a bath temperature of 12 K was demonstrated showing a 2150 K noise temperature and a 5 GHz NBW. At a bath temperature of 4.2 K the noise temperature reduced to 1700 K keeping a NBW of 5 GHz. The same 3.5 GHz GBW was measured for both bath temperatures. The voltage responsivity of such a device was estimated to be 1–2 kV/W at 1.6 THz. The results of preliminary noise measurements at a 2.6 THz LO as well as modeling of HEB conversion gain using the standard model are presented. Based on this research operation of MgB_2 HEB mixers with T_c >30 K at bath temperatures >20 K is suggested with no or acceptable sensitivity reduction.

Keywords: THz detectors, bolometers, mixers, MgB_2, superconductors, noise temperature, conversion gain, bandwidth.

List of Publications

Appended papers

This thesis is based on the following papers:

[A] S. Bevilacqua, **E. Novoselov**, S. Cherednichenko, H. Shibata and Y. Tokura, "MgB_2 hot-electron bolometer mixers at terahertz frequencies", in *IEEE Transactions on Applied Superconductivity*, vol.25, no.3, pp.2301104, June 2015.

[B] **E. Novoselov**, S. Bevilacqua, S. Cherednichenko, H. Shibata and Y. Tokura, "Noise measurements of the low T_c MgB_2 HEB mixer at 1.6 THz and 2.6 THz", in Proceedings of *26th International Symposium on Space Terahertz Technology*, 16-18 March 2015, Cambridge.

[C] **E. Novoselov**, S. Bevilacqua, S. Cherednichenko, H. Shibata and Y. Tokura, "Effect of the critical and operational temperatures on the sensitivity of MgB_2 HEB mixers", submitted to *IEEE Transactions on Terahertz Science and Technology*, 2015.

Other papers and publications

The following papers and publications are not appended to the thesis, either due to contents overlapping of that of appended papers, or due to contents not related to the thesis.

- [a] S. Cherednichenko, S. Bevilacqua and **E. Novoselov**, "THz hot-electron bolometer mixers", in *IEEE International Conference on Infrared, Millimeter and Terahertz Waves*, pp. 1-3, 14-19 September 2014, Tucson.
- [b] S. Cherednichenko, **E. Novoselov**, S. Bevilacqua, H. Shibata and Y. Tokura, "Study of MgB_2 HEB mixers vs the LO frequency and the bath temperature", in Proceedings of *26th International Symposium on Space Terahertz Technology*, 16-18 March 2015, Cambridge.
- [c] S. Bevilacqua, **E. Novoselov**, S. Cherednichenko, H. Shibata and Y. Tokura, "Wideband MgB_2 hot-electron bolometer mixers: IF impedance characterisation and modeling", submitted to *IEEE Transactions on Applied Superconductivity*, 2015.
- [d] N. Balbekin, **E. Novoselov**, P. Pavlov, V. Bespalov and N. Petrov, "Nondestructive monitoring of aircraft composites using terahertz radiation", in SPIE Proceedings of *Saratov Fall Meeting 2014: Optical Technologies in Biophysics and Medicine XVI; Laser Physics and Photonics XVI; and Computational Biophysics*, vol. 9448, pp. 94482D, March 2015.

Notations and abbreviations

Notations

α	Thermometer local sensitivity
β	Acoustic phonon transmission coefficient
B	Bandwidth
C	Heat Capacitance
C_0	Self heating parameter
c_e	Electron specific heat
c_p	Phonon specific heat
d	Material thickness
2Δ	Superconducting energy gap
ΔT	Temperature increase
ΔT_c	Superconducting transition width
ΔU_0	DC voltage response
f_g	Gain bandwidth frequency
f_{IF}	Intermediate frequency
f_n	Noise bandwidth frequency
G	Thermal conductance
G_d	Dynamic thermal conductance
G_e	Dynamic thermal conductance
G_{LNA}	IF chain gain
G_m	Mixer conversion gain
G_{tot}	Receiver conversion gain
$\hbar$	Dirac constant
I	Current
I_0	Bias Current
I_c	Critical current
J_c	Critical current density
k_B	Boltzmann constant
λ	Wavelength
L	Bolometer length
L_{opt}	Optical losses
N_{out}	Output noise power
P	Power
P_{IF}	Intermediate power
P_{LO}	Local oscillator power

P_s	Signal power
R	Resistance
R_L	Load resistance
R_0	Bolometer resistance
R_S	Sheet resistance
R_t	Thermometer resistance
R_v	Responsivity
R_{300}	Room temperature resistance
ρ_{300}	Room temperature resistivity
T	Temperature
T_b	Bolometer temperature
T_{bath}	Reservoir temperature
T_c	Critical temperature
T_{FL}	Thermal fluctuation noise
T_J	Johnson noise
T_{LNA}	Amplifier noise temperature
T_m	Mixer noise temperature
T_{opt}	Equivalent noise temperature of optical components
T_{out}	Mixer output noise temperature
T_p	Phonon temperature
T_{rec}	Receiver noise temperature
T_{REF}	Equivalent noise temperature at the reference state
θ	Electron temperature
τ	Bolometer time constant
τ_θ	Response time
τ_e	Effective bolometer time constant
τ_{ep}	Electron phonon interaction time
τ_{esc}	Phonon escape time
τ_{mix}	Mixer time constant
τ_{pe}	Phonon electron interaction time
u	Speed of sound
U	Voltage
U_0	Bias voltage
U_{LO}	Voltage amplitude of the local oscillator
U_s	Voltage amplitude of the signal
ω	Angular frequency
ω_i	Imaginary frequency
ω_{IF}	Intermediate angular frequency
ω_{LO}	Local oscillator angular frequency
ω_s	Signal angular frequency
W	Bolometer width
χ	Power exchange function
Z	Bolometer impedance

Abbreviations

Al_2O_3	Sapphire
Au	Gold
B	Boron
DC	Direct current
DSB	Double sideband
FIR	Far Infrared
GaAs	Gallium arsenide
GBW	Gain bandwidth
GHz	10^9 Hz
HDPE	High-density polyethylene
HEB	Hot electron bolometer
HPCVD	Hybrid physical chemical vapour deposition
IF	Intermediate frequency
IR	Infrared
InP	Indium phosphide
InSb	Indium antimonide
I-V	Current versus voltage
LHe	Liquid helium
LNA	Low noise amplifier
LO	Local oscillator
LSB	Lower sideband
MBE	Molecular beam epitaxy
Mg	Magnesium
MgB_2	Magnesium diboride
NbN	Niobium nitride
NbTiN	Niobium titanium nitride
NBW	Noise bandwidth
PLD	Pulsed laser deposition
RF	Radio frequency
R-T	Resistance versus temperature
SEM	Scanning electron microscope
Si	Silicon
SiC	Silicon carbide
SiN_x	Silicon nitride
SIS	Superconductor-insulator-superconductor tunnel junction
SSPD	Superconducting single-photon detector
SQUID	Superconducting quantum interference device
THz	10^{12} Hz
Ti	Titamium
USB	Upper sideband

Contents

Chapter 1

Introduction

The 0.1–10 THz part of the electromagnetic spectrum, lying between the microwave and infrared (IR) bands, is referred to as the terahertz (THz) range or the THz gap [1,2]. Despite technological difficulties, this region is of the great interest for medical imaging [3], security [4], communication [5] and Earth and Space science [6]. The THz range covers rotational lines from simple molecules and the ground state fine-structure lines from atoms and ions [7]. This presents the great interest for astronomy [8], because of the possibility to study physics and chemistry of galaxies, star-formation regions, the interstellar medium, comets, asteroids, outer planet atmospheres, etc.

In order to fully benefit from THz remote sensing, heterodyne receivers with their high spectral resolution ($\lambda/\Delta\lambda \approx 10^6$–$10^7$) are required [9]. Several types of devices might be used as a mixer element for a heterodyne receiver [10], e.g. Schottky diodes, Superconductor-insulator-superconductor tunnel (SIS) junctions, hot-electron bolometers (HEBs). A new class of low-noise heterodyne receivers based on superconducting HEB mixers was introduced [11] after the discovery of electron-heating effect in superconducting films [12]. Until recently, the state-of-the-art phonon-cooled HEBs were fabricated using niobium nitride (NbN) and niobium titanium nitride (NbTiN) ultra-thin films. HEB mixers have proved themselves to be highly sensitive THz detectors providing a low receiver noise temperature from 300 K at 1.3 THz local oscillator (LO) [13] to 1150 K at 5.3 THz LO [14]. HEB mixers were employed in many receivers for astronomical and atmospheric science observation programs launched in recent years, including RLT [15], APEX [16], [17], Herschel [18], [19], TELIS [20], [21], SOFIA [22], [23]. They were also chosen for various current programs, such as ASTE [24], DATE5 [13].

NbN HEB mixers typically have a gain bandwidth (GBW) of 3–4 GHz (NbTiN HEB mixers have even smaller GBW of ≈2 GHz). As a result, a receiver noise temperature increases towards higher intermediate frequencies (IFs) and doubles already at an intermediate frequency (IF) of 4–5 GHz. Therefore, the number of scientific tasks in sub-mm wave astronomy which can be performed with HEB mixers becomes limited [25].

Figure 1.1 shows a mapping of Galaxy M82 by the HIFI instrument of the Hershel Space Observatory [25]. The high spectral resolution and the high sensitivity of the HIFI instrument allowed for observation of very weak

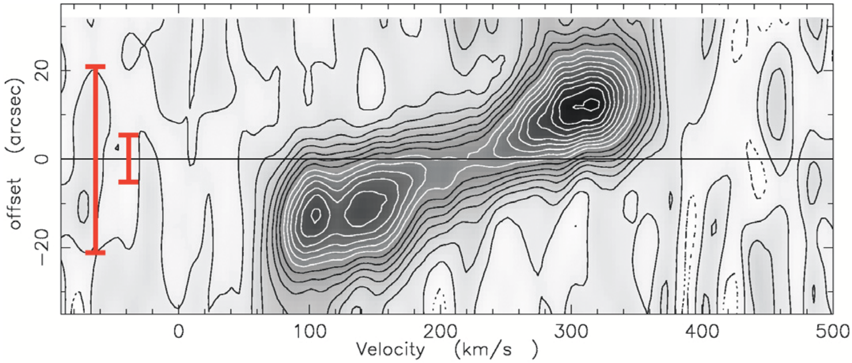

Fig. 1.1: Position-velocity diagram of the Nucleus of M82 mapped by the Hershel Space Observatory. The two red bars show the largest (44” at 0.57 THz) and smallest (12” at 1.9 THz) beams in observations [25].

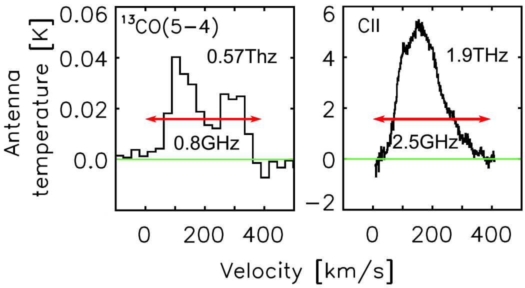

Fig. 1.2: Observed spectra of Galaxy M82 by the Hershel Space Observatory: CO line at 0.57 THz by SIS mixers (left) and CII line at 1.9 THz by HEB mixers (right). The same velocity range corresponds to about 3 time wider signal bandwidth at 1.9 THz then at 0.57 THz [25].

(<5 K) frequency-shifted emissions from the two arms of the galaxy. Measured spectra at two frequencies 0.57 THz (CO line) and 1.9 THz (CII line) are shown in Figure 1.2. One arm of the galaxy is moving towards us the other from us, which results in the existence of two main velocity components: the blue-shifted and the red-shifted emission lobes, which are clearly seen on the left spectrum in Figure 1.2. The large difference between the relative to the Earth velocities of the Galaxy M82 arms of 400 km/s resulted in a rather large IF bandwidth of about 2.5 GHz for the 1.9 THz CII spectral line. The nominal 2.4 GHz bandwidth of the used mixers was just enough to fit this spectral line, but it was not enough to get the baseline of the signal properly. At the same time, the observation at higher frequencies might be interesting due to the smaller beam size. For example, the beam at 1.9 THz was almost four times smaller than at 0.57 THz (red bars on Fig. 1.1). Moreover, emission lines for some molecules exist only at higher frequencies.

A superconducting critical temperature (T_c) of 8–11 K limits a NbN HEB mixer operation to the liquid helium (LHe) temperatures (<4.2 K). The lack of 4K cryocoolers qualified for space application necessitates utilization of LHe and leads to the reduction of spaceborn missions lifetimes.

The discovery of superconductivity in magnesium diboride (MgB_2) [26] with the highest T_c among intermetallic compounds (bulk T_c = 39 K) and fast progress in thin film deposition [27–29] opened new opportunities in HEB development. The first heterodyne mixing in a MgB_2 HEB with a T_c of 22 K made from a 20 nm thin film deposited on a silicon (Si) substrate using molecular beam epitaxy (MBE) [29] was reported in 2007 [30]. The device had a rather high receiver noise temperature of 11000 K at a 1.6 THz LO but the GBW was already 2.3 GHz at a 0.6 THz LO despite such a thick film. In subsequent works [31–33] a GBW of MgB_2 HEB mixers was mostly studied. A GBW of 3.4, 2.3 and 1.3 GHz at 0.35 and 0.6 THz LOs were measured for devices made from 10, 15 and 30 nm thin films, respectively, deposited on a c-cut sapphire (Al_2O_3) substrate by MBE [34]. The T_c of these devices were in range of 14–25 K depending on the film thickness. The big size of the HEBs (100–500 μm^2) and consequently high LO power requirement forced the use of low frequency (0.35–0.6 THz) sources as LOs where more power is available. Therefore, a large superconducting energy gap necessitated the use of high bath temperatures up to the few degrees below the T_c to make the gap smaller than the energy of photons of the LO. The GBW up to 8–10 GHz and the possibility of operation at bath temperatures >20 K were predicted for the MgB_2 HEB mixers made from 3–5 nm thin films with a T_c >30 K [32]. This prediction was proved later [35]: the GBW greater than 8 GHz at a 25 K bath temperature was demonstrated for a device with a T_c of 33 K made from a 15 nm film deposited on silicon carbide (SiC) using hybrid physical-chemical vapor deposition (HPCVD) [36]. However, the receiver noise temperature of this device was rather high 4000 K at a 0.6 THz LO.

Fabrication of smaller devices (3–42 μm^2) reduced the LO power requirement and allowed for the study of MgB_2 HEB mixers sensitivity in a wide range of bath temperatures [32, 33]. For a device with a T_c of 8.5 K the minimum receiver noise temperature was measured to be 800 K at a 0.6 THz LO with a GBW of 1.5 GHz at a 4.2 K bath temperature [32]. The minimum noise temperature of a HEB mixer with a T_c of 15 K was reported to be 1500 K at a 0.6 THz LO; authors have also demonstrated that it stays constant from 4.2 K up to 10.5 K bath temperature [33]. The need for fabrication of submicron size MgB_2 HEB mixers was noted for the possibility of operation at higher LO frequencies [33].

The motivation of the research presented in this thesis is the need for high sensitive heterodyne receivers operating at THz frequencies with a bandwidth superior to NbN HEB mixers. To achieve a sensitivity superior to NbN HEB mixers at bath temperatures above the LHe temperature, by fabrication of submicron size MgB_2 HEB mixers, and the study of their intrinsic parameters behaviour versus a bath temperature, is the main goal of this work.

The thesis is structured in 4 chapters. Chapter 2 contains an overview of: bolometer detection principles, heterodyne mixing, the standard model of superconducting HEBs, and MgB_2 HEB mixers. The HEB fabrication process using electron beam lithography, metal evaporation and ion-beam milling is presented in Chapter 3. The detailed description of the measurement setup and used techniques as well as experimental results are given in Chapter 4. Finally Chapter 5 summarises the results of this work and provides the future work overview.

Chapter 2

Background

This chapter provides an overview of: bolometer operation principles and main characteristics which determine the bolometer performance. Total power and frequency selective detection regimes of bolometer operation are described and discussed. The standard model of HEB is presented as well as some important properties of MgB_2 as a material for superconducting HEB mixers.

2.1 Bolometric receiver

A simple bolometer consists of three parts. Figure 2.1(a) represents these parts: an absorber where an incident power is absorbed and thermalized; a perfectly coupled thermometer which measures changes of the absorber temperature; and a weak thermal link connecting the absorber and a heat sink to return the absorber into the initial state in an absence of incident power. The absorber is characterised by a heat capacity C, the thermal link by a thermal conductivity G and the heat sink by a temperature T_{bath}.

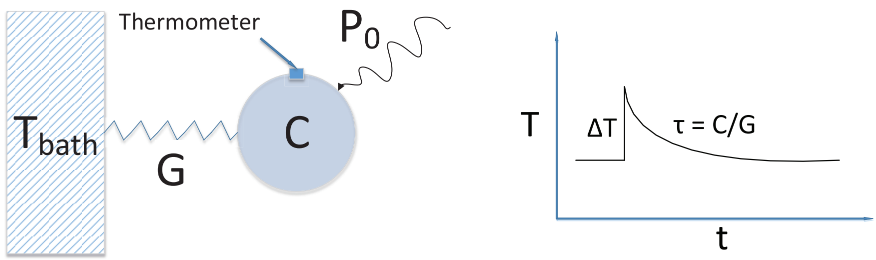

(a) (b)

Fig. 2.1: (a) A schematic of simple bolometer consisting of an absorber with a heat C, a thermometer and a weak link with a thermal conductivity G connecting the absorber to a heat sink with a temperature T_{bath}. (b) A schematic representation of bolometer working principe. An irradiation with an incident power P_0 increase a bolometer temperature by $\Delta T = P_0/G$. After the disappearance of radiation the bolometer temperature decay back with a time constant $\tau = C/G$.

This device can be used to measure a steady power input P_0 which gives a temperature increase of $\Delta T = P_0/G$ with an assumption of uniform heating of the bolometer. In case of a variable power P(t) the dynamics of the bolometer temperature T_b can be described by a heat balance equation:

$$C\frac{dT_b}{dt} + G(T_b - T_{bath}) = P(t) \tag{2.1}$$

When the bolometer is no longer irradiated, i.e. P(t)=0, its temperature relaxes back to T_{bath}. Then Equation 2.1 can be solved as:

$$T_b(t) = T_{bath} + \Delta T e^{-\frac{t}{\tau}} \tag{2.2}$$

where τ=C/G is a bolometer time constant. The time constant determines: in a total power detection regime how fast the bolometer is; in a frequency selective detection regime the bolometer IF bandwidth.

2.1.1 Total power detection

A schematic of total power detection principle is depicted in Figure 2.2. Being irradiated by the input power P_0 the receiver produces a DC voltage response ΔU_0 which is proportional to the power of incoming radiation. In this case the receiver measures the total power of incoming radiation independently on frequency in the whole band where the receiver is sensitive. In order to measure the input power in a certain band a narrowband filter might be placed at the receiver input, e.g. a Michelson interferometer. The maximum spectral resolution which might be achieved in this case is $\approx 10^3$. The total power detector is characterised by a voltage responsivity:

$$R_v = \frac{\Delta U_0}{P_0} \tag{2.3}$$

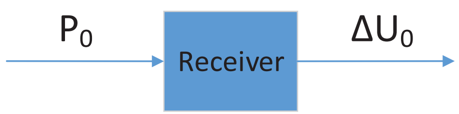

Fig. 2.2: A schematic of total power detection principle.

In case of the bolometer an electrical resistance thermometer (see Fig. 2.3) might be used to measure the temperature T_b. In the electrical resistance thermometer a change in temperature is converted into a change in resistance R which with a readout current is converted into voltage changes. The temperature of such a bolometer irradiated by the input power $P(t) = P_0 + P_1 e^{i\omega_s t}$ changes as $T_b = T_0 + T_1 e^{i\omega_s t}$.

The voltage responsivity of bolometer with a resistive thermometer biased with the readout current I_0 is [37]:

$$R_v = \frac{I_0 \frac{dR_t}{dT}}{G_d - I_0^2(\frac{dR_t}{dT}) + i\omega_s C} \tag{2.4}$$

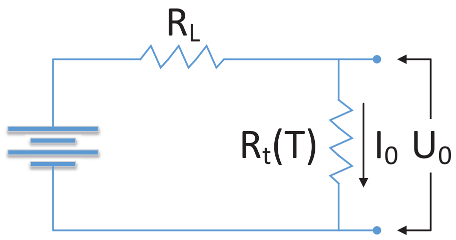

Fig. 2.3: A bias circuit of electrical resistance thermometer. I_0 is a bias current, U_0 is a bias voltage, R_L is a load resistance, $R_t(T)$ is a temperature dependent thermometer resistance.

where G_d=dP/dT is a dynamic thermal conductance at the temperature T_0. Equation 2.4 is valid if the resistance of the load resistor $R_L \gg R_t$. The responsivity of the bolometer is influenced by a thermal feedback which can be expressed as the effective thermal conductance G_e=G_d-I^2(dR_t/dT). The thermal feedback also modifies the measured bolometer time constant τ_e=C/G_e. It is convenient to define a local sensitivity for the thermometer α=R_t^{-1}(dR_t/dT) evaluated at T_0. With new definitions the voltage responsivity becomes:

$$R_v = \frac{I_0 R_t \alpha}{G_e(1 + i\omega_s\tau_e)} \tag{2.5}$$

2.1.2 Frequency selective detection

The frequency selective detection has some advantages over the total power detection. First, amplitude information as well as phase information of incoming radiation is preserved. Second, a narrowband filter is not required at the receiver input while a high spectral resolution is achieved.

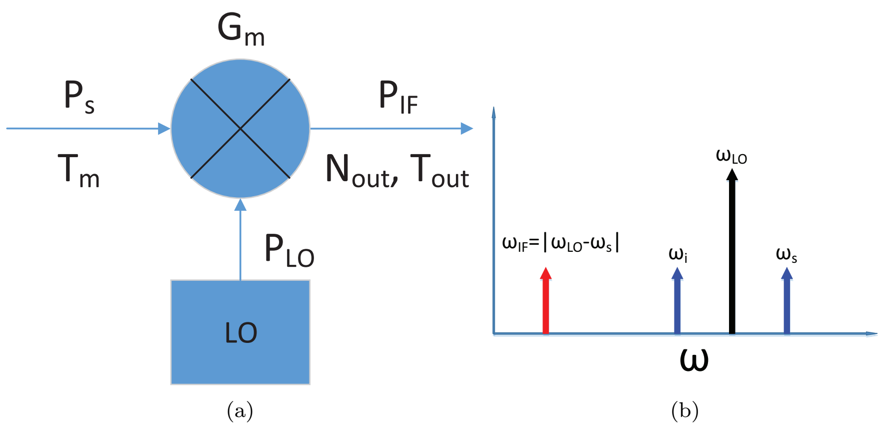

Fig. 2.4: (a) A schematic of down-converting mixer. (b) A schematic of down-conversion in a frequency domain.

In this case the bolometer work as a down-converting mixer which mix an incident signal (ω_s), which in a general case might be represented as a sum of frequency components, with a LO (ω_{LO}) (see Fig. 2.4). The total RF voltage across the bolometer U(t) would be:

$$U(t) = U_s(cos(\omega_s t)) + U_{LO}(cos(\omega_{LO} t)) \tag{2.6}$$

where U_s and U_{LO} are amplitudes of signal and LO voltages, respectively, at the bolometer input. The total power dissipated in the bolometer is:

$$P(t) = \frac{U(t)^2}{2R} \tag{2.7}$$

Inserting Equation 2.6 into 2.7 and taking into account that the bolometer temperature can not follow high frequency terms $2\omega_s$, $2\omega_{LO}$ and $\omega_s + \omega_{LO}$ the total dissipated power becomes:

$$P(t) = P_s + P_{LO} + 2\sqrt{P_s P_{LO}} cos(\omega_{IF} t) \tag{2.8}$$

where $P_s = U_s^2/2R$, $P_{LO} = U_{LO}^2/2R$ and $\omega_{IF} = |\omega_s - \omega_{LO}|$ which should be less then $1/\tau_e$. As it follows from Equation 2.8 the IF output P_{IF} at a frequency ω_{IF} can be produced by either an Upper Sideband (USB) $\omega_s = \omega_{LO} + \omega_{IF}$ or a Lower Sideband (LSB) $\omega_i = \omega_{LO} - \omega_{IF}$ (see Fig. 2.4(b)). Mixers sensitive to both USB and LSB are called Double Sideband (DSB). The performance of mixer is characterised by a mixer conversion gain:

$$G_m = \frac{P_{IF}}{P_s} \tag{2.9}$$

Another important figure of merit for the mixer is a noise. The mixer itself produce the noise at the output with a power N_{out}. This noise might be represented with the output noise temperature T_{out} using the Johnson-Nyquist equation:

$$T_{out} = \frac{N_{out}}{k_B B} \tag{2.10}$$

where k_B is the Boltzmann constant and B is a bandwidth. Using the mixer conversion gain the output noise temperature T_{out} might be referred to the mixer input in case of DSB mixer as:

$$T_m = \frac{T_{out}}{2G_m} \tag{2.11}$$

2.2 HEB mixers

The term "hot electrons" is used to describe a non-equilibrium state of electrons inside the bolometer, i.e. an effective elevation of electron temperature. The first HEB mixer was realised using a doped semiconductor indium antimonide (InSb) [38]. Despite a good sensitivity, the devices based on InSb had quite a small bandwidth due to time constants of the microsecond order [39]. After the discovery of electron-heating effect in superconducting films [12] superconductors emerged as a material for HEB mixers [11]. The resistance of a superconductor is strongly affected by the electron temperature in a region close to a T_c, which explains the HEBs' high sensitivity. HEB mixers made from NbN films were successfully implemented [40] allowing for the achievement of a typical bandwidth up to 4 GHz [41].

2.2.1 Photo response of phonon-cooled HEB mixers

Two types of superconducting HEB mixers differing by the dominating mechanism of electron cooling were reported: phonon-cooled [11] and diffusion-cooled [42]. In a phonon-cooled HEB a thin superconducting film deposited on a substrate plays a role of an absorber. The film cools down through the substrate, which plays a role of a heat sink. A thermal link between them is a thermal boundary resistance. The superconducting film acts also as a resistive thermometer. The thermalisation scheme of such a device is depicted in Figure 2.5.

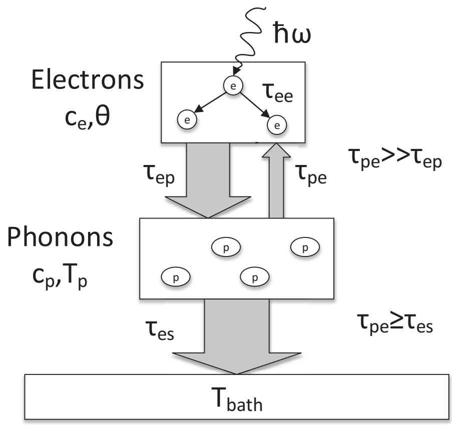

Fig. 2.5: Energy transfer and intrinsic relaxation times in a phonon-cooled HEB [43].

In order to operate as a receiver the HEB is cooled down below its T_c where a thermal coupling between phonons and electrons is week and the electron-electron interaction is strong. The interaction time between electrons τ_{ee} is shorter than other characteristic time constants, which makes possible to present the HEB as a two-temperature system. The first (electron) subsystem consists of quasiparticles and has a temperature θ and a specific heat c_e. The second (phonon) subsystem is formed by phonons in a superconducting film and has a temperature T_p and a specific heat c_p. The heat exchange between electron and phonon subsystems is done with characteristic time constants τ_{ep} and τ_{pe}. In an equilibrium state this interaction times relates as $\tau_{pe} = \tau_{ep}c_p/c_e$ and in order to achieve electron cooling τ_{ep} should be less then τ_{pe}. Then instead of one heat balance equation 2.1 a system of heat balance equations might be written as [44]:

$$c_e \frac{d\theta}{dt} = P(t) - c_e \frac{\theta - T_p}{\tau_{ep}} \tag{2.12}$$

$$c_p \frac{dT_p}{dt} = c_e \frac{\theta - T_p}{\tau_{ep}} - c_p \frac{T_p - T_{bath}}{\tau_{esc}} \tag{2.13}$$

where τ_{esc} is an escape time of phonons from the superconducting film into the substrate:

$$\tau_{esc} = \frac{4d}{\beta u} \tag{2.14}$$

where d is a superconductor thickness, u is a speed of sound and β is an acoustic phonon transmission coefficient. The phonon escape time τ_{esc} should be less then the electron-phonon interaction time τ_{ep} to prevent heat accumulation in the phonon subsystem. The reverse energy flow carried by the phonons from the substrate into the superconductor is neglected. In the low temperature limit when c_e is much larger then c_p the electron temperature relaxation could be described with a single time constant τ_θ [45]:

$$\tau_\theta = \tau_{ep} + \tau_{esc}\frac{c_e}{c_p} \tag{2.15}$$

while in a general case a relation between τ_θ, τ_{ep} and τ_{esc} is more complicated [44].

As it is seen from Equation 2.14 it is required to reduce the film thickness to achieve the shorter phonon escape time. Unfortunately, the reduction of film thickness lead to a reduction of T_c, e.g. due to a large amount of defects in a film bottom layer. NbN with a bulk T_c of 16 K has only a 8–11 K T_c in 3–5 nm films.

2.2.2 The HEB standard model

In order to analyze the HEB behavior the standard model previously developed for NbN HEBs [11] might be used. The model assumes that the electron temperature along the superconducting film is uniform and radio frequency (RF) radiation and a direct current (DC) power have the same effect on the HEB. However, this assumption was not completely true and development of the hot-spot models [46–48] was required. In the hot-spot models the electron temperature profile inside the superconducting film was taken into account. Compared to the standard model modifications of heat balance equation were done. This modifications allowed for the correct modeling of HEB noise and current versus voltage (I-V) curves, while the standard model requires experimental curves for modeling.

2.2.2.1 HEB conversion gain

Using standard lumped element formalism expression for the HEB voltage responsivity might be written as [49]:

$$R_v(f_{IF}) = \frac{R_L I_0}{R_L + R_0}\frac{\frac{C_0}{\chi}}{1 - C_0 I_0^2 \frac{R_L - R_0}{R_L + R_0}}\frac{1}{1 + i\frac{f_{IF}}{f_g}} = R_v(0)\frac{1}{1 + i\frac{f_{IF}}{f_g}} \tag{2.16}$$

where R_0 is the HEB DC resistance at the bias point, f_g is the HEB 3dB gain roll-off frequency (GBW) and C_0=dR/dP is a self-heating parameter (P is a sum of dissipated DC and LO powers). An assumption that the impedance of a HEB at the high-frequency limit $Z(\infty)$ is equal to R_0 was done. For Nb HEBs it was shown that a real part of $Z(f_{IF})$ goes to R_0 at frequencies >1 GHz [50]. For MgB_2 HEBs a similar investigation on the IF impedance was performed recently [51]. It was shown that a real part of HEB impedance approaches differential resistance dU/dI at low frequencies and R_0 at higher frequencies similar to NbN HEBs [52]. A power exchange function χ is introduced in a similar way as in [53]. It is defined as a ratio of the RF and DC power changes required to keep the device resistance constant. As a general rule a HEB resistance is more sensitive to a DC power then to an RF power, which results in conversion functions larger than one. It was demonstrated that χ typically takes values from 3 to 1 decaying moving to higher biases [47, 52]. The mixer conversion gain is given by [49]:

$$G_m(f_{IF}) = \frac{2P_{LO}R_v^2(f_{IF})}{R_L} \tag{2.17}$$

where P_{LO} is an absorbed LO power.

Inserting Equation 2.16 into 2.18 the mixer conversion gain predicted by the standard model is calculated as:

$$G_m(f_{IF}) = \frac{2P_{LO}R_L I_0^2}{(R_L+R_0)^2} \frac{(\frac{C_0}{\chi})^2}{(1-C_0 I_0^2 \frac{R_L-R_0}{R_L+R_0})^2} \frac{1}{1+(\frac{f_{IF}}{f_g})^2} = G_m(0)\frac{1}{1+(\frac{f_{IF}}{f_g})^2} \tag{2.18}$$

where $G_m(0)$ is a mixer conversion gain at zero IF.

Another assumption made in this theory is that the resistance of HEB depends on the electron temperature. Since the temperature is linearly proportional to the dissipated power $R=C_0P$. After some mathematical derivations it was shown that [50]:

$$C_0 = \frac{1}{I_0^2}\frac{\frac{dU}{dI}-R_0}{\frac{dU}{dI}+R_0} \tag{2.19}$$

2.2.2.2 HEB noise temperature

The main noise sources in a HEB mixer are Johnson and thermal fluctuation noises [11]. Output noise temperatures T_J and T_{FL} produced by the each noise component might be calculated [54] according the Mather's nonequilibrium theory of bolometer detector [55] as:

$$T_J(f_{IF}) = \frac{4R_L R_0 \theta}{(R_L+R_0)^2(1-C_0 I_0^2 \frac{R_L-R_0}{R_L+R_0})^2} \tag{2.20}$$

$$T_{FL}(f_{IF}) = \frac{I_0^2 R_L (\frac{\partial R}{\partial \theta})^2 \frac{4\theta^2}{c_e V}\tau_\theta}{(R_L+R_0)^2(1-C_0 I_0^2 \frac{R_L-R_0}{R_L+R_0})^2} \frac{1}{1+(2\pi f_{IF}\tau_\theta^*)^2} \tag{2.21}$$

where V is a device volume and τ_θ^* is the electron temperature relaxation time modified by the electro-thermal feedback:

$$\tau_\theta^* = \frac{\tau_\theta}{1-C_0 I_0^2 \frac{R_L-R_0}{R_L+R_0}} \tag{2.22}$$

The DSB mixer input noise temperature which also include a noise from an IF chain T_LNA is [54]:

$$T_m(f_{IF}) = \frac{T_J + T_{FL} + T_{LNA}}{2G_m(0)(1+(\frac{f_{IF}}{f_g})^2)^{-1}} \tag{2.23}$$

The thermal fluctuation noise depends on the IF as $(1+(2\pi\ f_{IF}\ \tau_\theta^*)^2)^{-1}$. Since τ_θ^* and a mixer time constant $\tau_{mix}=(2\pi\ f_g)^{-1}$ basically are equal, Equation 2.23 could be rewritten as:

$$T_m(f_{IF}) = \frac{T_{FL}(0) + (T_J + T_{LNA})\ (1 + (\frac{f_{IF}}{f_g})^2)}{2G_m(0)} \tag{2.24}$$

And then defining a new parameter f_n as a mixer noise bandwidth (NBW):

$$f_n = f_g\sqrt{\frac{T_{FL} + T_J + T_{LNA}}{T_J + T_{LNA}}} \tag{2.25}$$

the final equation becomes:

$$T_m(f_{IF}) = T_m(0)\ (1 + (\frac{f_{IF}}{f_n})^2) \tag{2.26}$$

where $T_m(0)$ is a mixer noise temperature at zero IF.

2.2.3 MgB_2 HEB mixers

The superconductivity of MgB_2 was reported in 2001 [26] and immediately encouraged a great interest to MgB_2 film deposition [27–29]. The significant progress in thin MgB_2 film deposition allowed for fabrication of different types of superconducting devices, e.g. HEB mixers [30], superconducting single-photon detectors (SSPD) [56], superconducting quantum interface devices (SQUID) [57].

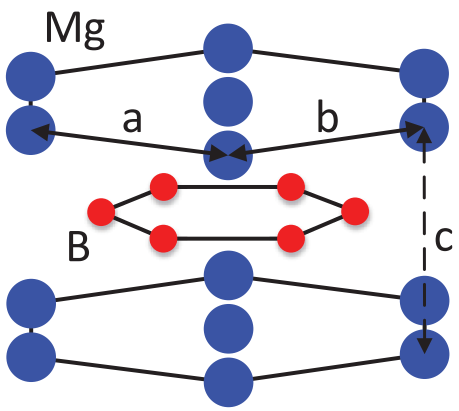

Fig. 2.6: MgB_2 crystal structure. Honeycomb boron layers are in between of hexagonal magnesium layers [26].

MgB_2 is a conventional intermetallic compound superconductor with the highest T_c of 39 K reported so far. The crystal structure of MgB_2 is shown in Figure 2.6. It consists of hexagonal magnesium (Mg) layers and honeycomb boron (B) layers in between. The hexagonal unit cell has the following lattice parameters a=b=3.086 Å, c=3.524 Å [26]. MgB_2 is a conventional BCS superconductor. However, it exhibits a double superconducting gap structure with $2\Delta_\sigma \approx 4k_BT_c$ and $2\Delta_\pi \approx 1.3k_BT_c$ [58]. In the dirty limit, due to strong interband and intraband scattering two superconducting gaps merges into one energy gap $2\Delta_{dirty}$ which temperature dependance deviates from BCS curve [59].

Several methods for deposition of thin MgB_2 films were realised, e.g. pulsed laser deposition (PLD) [27], MBE [29], HPCVD [28]. The most suitable substrates for MgB_2 thin film deposition are Al_2O_3 and SiC with a lattice mismatch with MgB_2 of $\sim$11% (30° in-plane rotation) [60] and $\sim$0.42% [61], respectively.

MgB_2 thin films are very attractive for HEB fabrication. The shorter, in comparison to NbN (12 ps), electron-phonon interaction time was measured in a thin MgB_2 film on a Si substrate (3 ps) [58]. The possibility of very thin film deposition (6–8 nm) with a high T_c of 34–41 K was demonstrated [61, 62]. This facts indicates a potential to achieve a wider IF bandwidth and higher operation temperatures compared to NbN HEB mixers. The recent results for MgB_2 HEB mixers were achieved with devices fabricated from MBE deposited films on Al_2O_3 [31–33] substrates and HPCVD deposited films on SiC substrates [35, 63].

Chapter 3

MgB_2 HEB fabrication process and DC characterisation

Several batches of submicrometer size HEBs were fabricated using electron beam lithography, ion beam milling and lift-off process. The fabrication of the devices was quite challenging. In order to match HEBs to the 90 Ω spiral antenna they should be short and wide due to a high resistivity of available MgB_2 films. A reduction of the bolometer width down to 1 μm necessitates a decrease of the length down to 0.2 μm. In addition, since MgB_2 degrades during exposure to water and oxygen [64, 65], the processing must provide protection to preserve the quality of the MgB_2 films.

In this chapter the detailed description of the device fabrication process and the DC test results are presented.

3.1 Device fabrication

The HEBs were fabricated using MgB_2 films provided by NTT Basic Research Laboratories. Films were deposited on a c-cut Al_2O_3 substrate by MBE [66]. Typically the T_c of MBE films is much lower than that of HPCVD films, but the film surface is smoother, which is essential for the device fabrication and performance. The film deposition process included co-evaporation of Mg and B in a highvacuum chamber at 280° and subsequent Ar atmosphere annealing in a rapid-annealing furnace. All films were covered *in-situ* with a 20 nm gold layer to reduce contact resistance between a MgB_2 film and metal layers deposited later and to prevent film degradation during storage and initial HEB fabrication steps.

The HEB chip design is given in Figure 3.1. Several types of integrated planar antennas might be used with HEB mixers, e.g. a twin-slot antenna [67], a slot-ring antenna [68], a log-periodic antenna [69] and a spiral antenna [70]. The spiral antenna is the most suitable antenna type for device testing at different frequencies. It provides a broad band and frequency independent impedance.

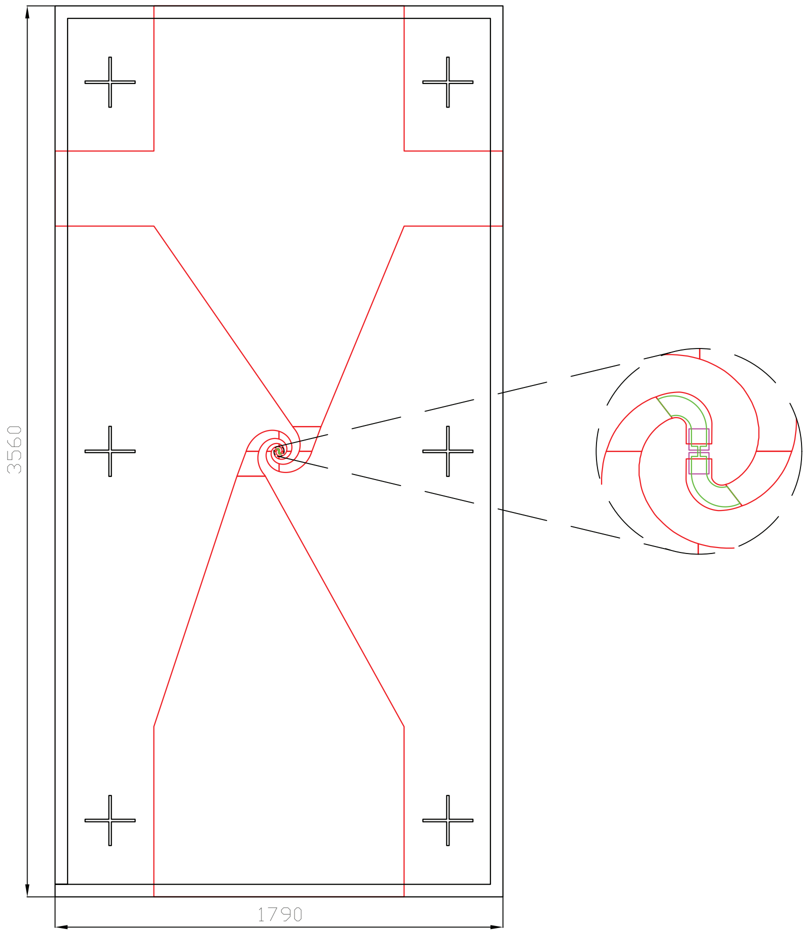

Fig. 3.1: The design of MgB_2 HEB mixer including alignment marks. The sizes are given in microns.

The HEBs were fabricated using e-beam lithography, argon ion beam milling and lift-off process in several steps:

1. **Alignment marks and chip frames**: Initially, alignment marks for pattern alignment at subsequent processing steps and chip frames for short circuiting bolometers, to avoid possible device damaging by the electrostatic charge, were fabricated. After the e-beam lithography, metal evaporation (10nm Ti, 150nm Au and 30nm Ti) and lift-off were performed. The top Ti layer was used to protect structures during ion beam milling at following steps.

2. **Contact pads**: Contact pads defining the bolometer lengths were patterned. After the e-beam lithography, metal evaporation (10 nm Ti, 100 nm Au and 30 nm Ti) and lift-off were performed.

3. **Antennas**: The broadband planar spiral antennas for radiation coupling

into the HEBs were patterned. The antenna center parts were overlapping with the contact pads. After the e-beam lithography, metal evaporation (10 nm Ti, 270 nm Au and 30 nm Ti) and lift-off were performed.

4. **Etching and passivation**: At this stage the 20 nm thick *in-situ* Au layer was etched away using Ar ion beam milling. To prevent the degradation of the MgB_2 film during the rest of the processing steps, immediately after the etching, the devices were passivated with 40 nm thick SiN_x film by RF magnetron sputter.

5. **Width definition and etching**: For the bolometer widths definition etching masks were patterned using negative e-beam resist. The SiN_x passivation and MgB_2 film were etched away except from the bolometer area protected by the resist.

6. **Dicing**: Finally, the wafer was cut into $1.7\times3.5\,\mathrm{mm}^2$ chips with the diamond dicing saw along the frame lines.

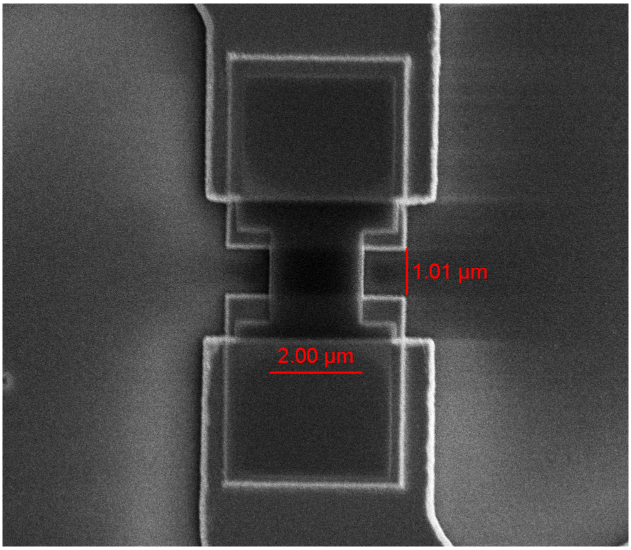

Fig. 3.2: SEM picture of one of the fabricated devices.

The scanning electron microscope (SEM) picture of one of the fabricated devices is presented in Figure 3.2. Since in a SEM an object is exposed to an electron beam and the probability to destroy it is high the chosen HEB was not used for RF testing.

For the batch B14 a 10 nm film was used, for the batches N1 and N3 20 nm films were used. Each substrate held eight HEBs of various dimensions. For 20 nm films all devices survived during the processing and dicing. For a 10 nm film, the yield was quite low and just a few devices were useful.

3.2 DC characterisation

Before performing RF characterisation, DC tests were conducted. One device from each of the three batches B14, N1, N3 was chosen for tests (see Table 3.1). HEB#1 discussed below was 10 nm thick and $1\times1\,\mu m^2$ in size with a T_c of 8.5 K. HEB#2 was 20 nm thick and $1\times0.2\,\mu m^2$ in size with a T_c of 22.5 K. HEB#3 was 20 nm thick and $1\times0.5\,\mu m^2$ in size with a T_c of 22 K. The resistance versus temperature (R-T) curves (see Fig. 3.3) were measured in a dip-stick for all HEBs. The devices were biased at a constant current (typically 10 μA) and cooled down from room temperature (300 K) to the LHe temperature (4.2 K). The presence of the double transition for HEB#2 and HEB#3 R-T curves (see the inset in Figure 3.3) suggests that the electrical contact between MgB_2 and Au was rather good (the proximity effect) [71]. The presented HEBs had different sizes, so the sheet resistance was calculated over different areas. Both the surface roughness and the inhomogeneity of film starts to play a more significant role when scaling the size to a submicron dimension, which resulted in an order of magnitude higher sheet resistance for the 20 nm devices. The resistivity measured in HEB#2 and HEB#3 is also an order of magnitude higher then the value reported for the 20 nm MBE films ($100–200\,\mu\Omega \times cm$) [66]. Moreover, 10 nm and 20 nm films were from different batches deposited under different conditions, which affected the film structure.

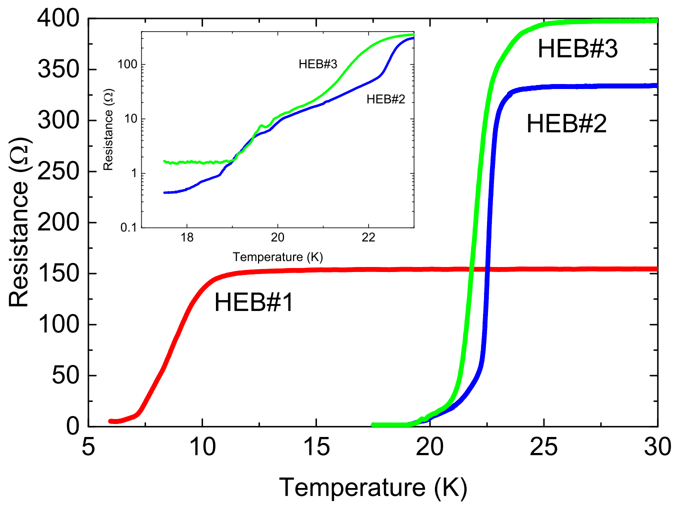

Fig. 3.3: Resistance versus temperature dependence for HEB#1, HEB#2 and HEB#3. Resistance in logarithmic scale for HEB#2 and HEB#3 is plotted in the inset.

At a bath temperature of 4.2 K I-V curves were recorded by sweeping the voltage as presented in Figures 3.4(a) and 3.4(b). Measured critical currents and obtained critical current densities are summarised in Table 3.1. HEB#1 had much smaller critical current density then two other devices, which together with a lower T_c suggests poorer film quality. The critical current den-

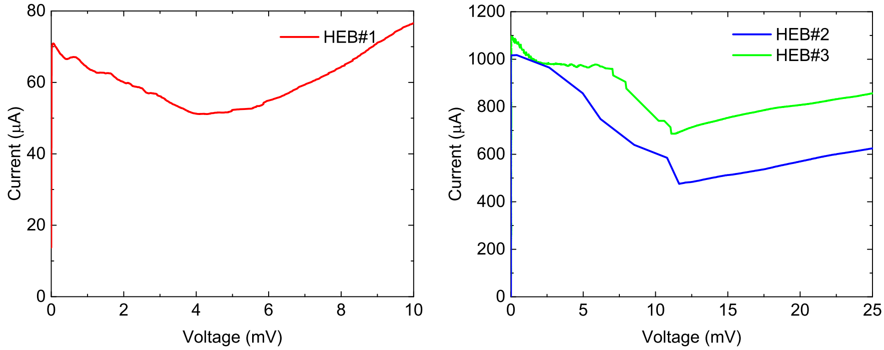

(a) (b)

Fig. 3.4: (I-V curves of (a) HEB#1 and (b) HEB#2 and HEB#3. HEBs at 4.2 K bath temperature.

sity of HEB#1 is in the same ballpark as values reported for the devices of similar size [33]. While the critical current densities of HEB#2 and HEB#3 are in order of magnitude higher because of the rapid annealing used for the film fabrication [66].

The results of DC measurements are very different from the data acquired with devices fabricated from HPCVD deposited films [72]. The resistivity of these 10–20 nm films was much smaller (20–40 $\mu\Omega \times cm$). The critical current density was also higher: 1–3 MA/cm^2 in 10–20 nm films already at 10 K.

A high T_c of 22-23 K according the BCS theory corresponds to a 8 meV σ band (or 1.9 THz, $2\Delta = \hbar\omega$, where $\hbar$ is the Dirac constant), where a conduction prevails for dirty samples [73, 74]. However, at a 1.6 THz LO the switching similar to the one of NbN devices under the pumping at frequencies below the superconducting gap frequency was not observed. It was demonstrated experimentally, that for the MgB_2 thin film with even higher T_c of 33 K the absorption of the radiation appears in a superconducting gap of 1.3 THz [75].

Table 3.1: MgB_2 HEB THICKNESS (d), SIZE (W×L), CRITICAL TEMPERATURE (T_c), TRANSITION WIDTH (ΔT_c), RESISTANCE AT 300 K (R_{300}), SHEET RESISTANCE (R_S), RESISTIVITY (ρ_{300}), CRITICAL CURRENT AT 4.2 K (I_c) AND CRITICAL CURRENT DENSITY (J_c)

Device	Batch	d(nm)	W×L(μm^2)	T_c(K)	Δ T_c(K)
HEB#1	B14	10	1×1	8.5	2.5
HEB#2	N3	20	1×0.2	22.5	0.6
HEB#3	N1	20	1×0.5	22	1.5

Device	R_{300} (Ω)	R_S (Ω/□)	$\rho_{300}(\mu\Omega \times cm)$	$I_c(\mu$A)	J_c(MA/cm^2)
HEB#1	160	160	160	70	0.7
HEB#2	330	1650	3300	1000	5
HEB#3	400	850	1700	1100	5.5

Some other batches (N2, N4 and N5) have been also fabricated using 10 nm and 40 nm films. The testing of these devices is within the scope of future research. The 10 nm HEBs have a higher T_c of 12–15 K in comparison with HEB#1 presented in this work. The 40 nm HEBs have a T_c of 29–30 K and can be tested at bath temperatures >20 K. However, the critical currents in these devices are rather high (18–20 mA), which can cause problems with pumping because of limited LO power available at high frequencies.

Chapter 4

MgB_2 HEB THz characterisation and modeling

This chapter describes THz characterisation of MgB_2 HEB mixers. The experimental data are presented as well as analysis using the standard model.

4.1 Experimental setup

HEB#1 was mounted in a mixer block with a 12 mm Si lens (see Fig. 4.1(a)) and placed on the LHe cryostat's cold plate. Elliptical Si lenses were used in order to improve radiation coupling. For HEB#2 and HEB#3 a different mixer block with a 5 mm Si lens was used (see Fig. 4.1(b)), and a parabolic off-axis mirror was placed inside the cryostat to focus an incident radiation into the device as shown in Figure 4.2.

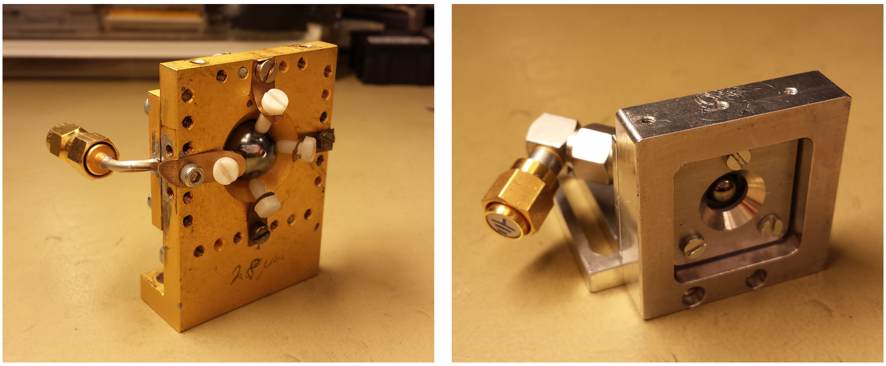

(a) (b)

Fig. 4.1: Mixer blocks used for (a) HEB#1 and (b) HEB#2 and HEB#3.

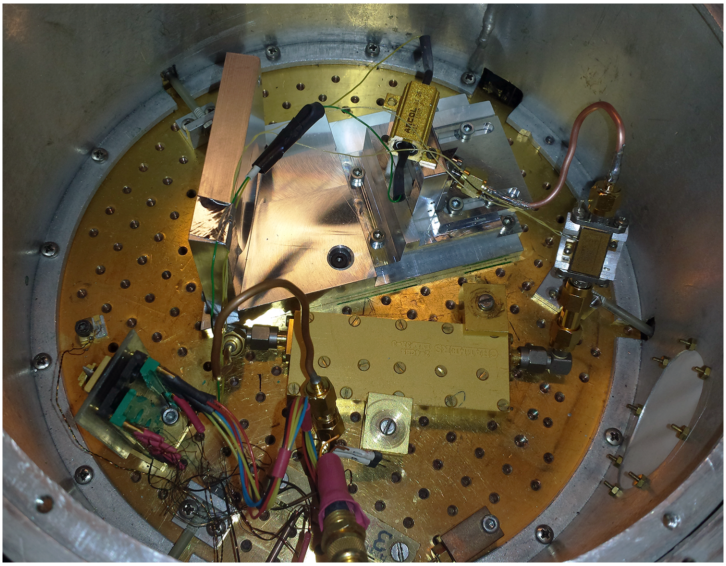

Fig. 4.2: The cold plate of LHe cryostat.

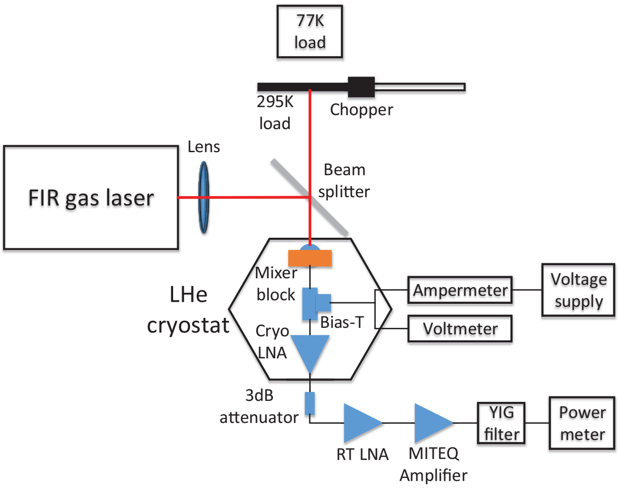

Fig. 4.3: The noise and gain measurement setup.

A Zitex™ IR filter was mounted on the 4K shield of the cryostat. A bias-T followed the mixer block to apply a voltage bias to the device and to separate an IF response (see Fig. 4.2). Several amplifiers were used in the IF chain to measure the IF response: the Chalmers 2–4 GHz InP low-noise amplifier (LNA) mounted on the cryostat's cold plate, the Chalmers 2–4 GHz GaAs LNA at room temperature outside the cryostat and the broadband 0.1–10 GHz MITEQ amplifier at the end.

The scheme of the experimental set-up is presented in Figure 4.3. A LO beam was focused by the Teflon lens and combined with signal beams from the hot/cold loads (Eccosorb sheets) using the Mylar® beam splitter. The high-density polyethylene (HDPE) window (not presented in Fig. 4.3) let incoming radiation enter the cryostat. The 3dB attenuator was placed between the cryostat and the first room temperature LNA to reduce a standing wave formation in the long IF cable. An amplified IF signal was measured through the tunable YIG-filter (50MHz bandwidth) with the powermeter. For direct detection experiments the cryostat was placed just in front of the far-infrared (FIR) gas laser front panel and the lock-in amplifier with the separate voltage pre-amplifier was used at the mixer bias line to detect amplitude modulated small signals.

Most of the noise and gain measurements were performed at a 1.6 THz LO, but some preliminary results at a 2.6 THz LO were also acquired for HEB#1. The Golay cell connected to the oscilloscope (not presented in Fig. 4.3) was placed behind the beam splitter to monitor a FIR gas laser emission power during experiments. Various bath temperatures were used during tests. The temperature of boiling LHe under the standard conditions (4.2 K) were used as a base temperature. To decrease a bath temperature down to 2.7 K a pumping of helium vapour was done. To increase a bath temperature up to 12 K the resistive heater mounted on the mixer block was used (see Fig. 4.2).

4.2 Noise and gain measurement techniques

Mixer radiometer sensitivity is a ability to detect small variations of the incoming THz radiation. The figure of merit for it is a DSB receiver input noise temperature. Since THz superconducting mixers (e.g. HEB mixers) are characterized in complex set-up contributions of all other components have to be analyzed. This would allow for de-embedding of the mixer input noise temperature.

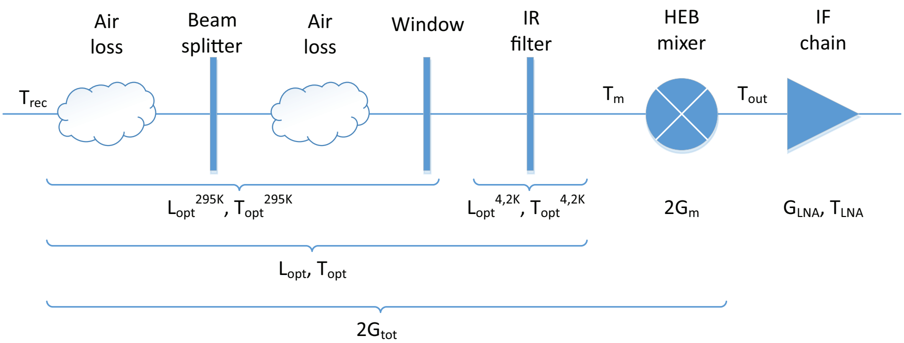

Fig. 4.4: The Losses and equivalent noise temperatures of optical and electrical components in the signal path.

Figure 4.4 represents the signal path through the optical and electrical components in the receiver. A contribution of optical elements to a noise temperature can be calculated using the general formula for lossy components

Table 4.1: LOSSES (L) AND EQUIVALENT NOISE TEMPERATURE (T_{eq}) OF OPTICAL COMPONENTS ALONG THE SIGNAL PATH REFERRED TO THE INPUT OF THE CORRESPONDING COMPONENT. T IS THE PHYSICAL TEMPERATURE OF THE COMPONENT.

Component	T(K)	L(dB)	T_{eq}(K)
Air path (40 cm)	295	1	76.4
Beam splitter (Mylar®)	295	0.1	7.0
Cryostat's window (1 mm HDPE)	295	0.7	52.5
IF filter (2 Zitex™ sheets)	4.2	0.6	0.6
Total	-	2.4	137

T_{eq}=(L-1)T (where L is a component loss and T is a physical temperature of component) and then deducted from a measured noise temperature (Table 4.1). The loss in the Si lens were treated as a part of mixer loss and was not deducted from a noise temperature. The DSB receiver noise temperature then is:

$$T_{rec} = T_{opt} + T_m L_{opt} + \frac{T_{LNA}}{2G_{tot}} \tag{4.1}$$

In order to measure the DSB receiver noise temperature T_{rec} the standard Y-factor technique was used. Y is a ratio of receiver output powers with hot and cold loads (in this case 295 K and 77 K, respectively):

$$Y = \frac{P_{hot}}{P_{cold}} = \frac{2G_{tot}G_{LNA}k_B(T_{rec} + T_{295K})B}{2G_{tot}G_{LNA}k_B(T_{rec} + T_{77K})B} = \frac{T_{rec} + T_{295K}}{T_{rec} + T_{77K}} \tag{4.2}$$

A noise temperature then becomes:

$$T_{rec} = \frac{T_{295K} - Y \times T_{77K}}{Y - 1} \tag{4.3}$$

In order to measure the mixer conversion gain (G_m) and the output noise temperature (T_{out}) the U-factor technique was applied [76]. The U-factor is defined as a ratio of a receiver output power when the receiver is in an operating state to an output power in a reference state which can be characterized by an equivalent temperature T_{REF}. As a reference state either a superconducting state or a normal state might be used. In a superconducting state a HEB works as a microwave short and reflects all power coming from an IF chain (T_{REF}=T_{LNA}, where T_{LNA} is an IF chain noise temperature). A normal state could be achieved by a heavy pumping of HEB with a LO. For a HEB in a normal state an output power is determined mostly by a thermal noise with an effective temperature which is equal to an electron temperature of HEB in this state (i.e. about a T_c). In both cases in a reference state an output power of receiver is determined by a sum of reference and IF chain noise temperatures:

$$U = \frac{2\ G_{tot}\ (T_{rec} + T_{295K})}{T_{LNA} + T_{REF}} \tag{4.4}$$

where G_{tot} is a receiver conversion gain (G_{tot} = G_m/L_{opt}; L_{opt} is an optical loss (in this case 2.4dB), G_m is a mixer conversion gain). A factor "2" in

Equation 4.4 comes from a DSB operation of HEB mixer and an assumption that a sideband ratio is one. In this case the mixer conversion gain might be calculated as:

$$G_m = G_{tot}\ L_{opt} = \frac{U\ (T_{LNA} + T_{REF})}{2\ (T_{rec} + T_{295K})} L_{opt} \tag{4.5}$$

Equation 4.4 could be modified to:

$$U = \frac{T_{out} + T_{LNA} + 2\ G_{tot}\ (T_{opt} + T_{295K})}{T_{LNA} + T_{REF}} \tag{4.6}$$

where T_{opt} is a noise contribution of optical components (in this case 137 K). Finally, the mixer output noise temperature becomes:

$$T_{out} = U\ (T_{LNA} + T_{REF}) - T_{LNA} - 2\ G_{tot}\ (T_{opt} + T_{295K}) \tag{4.7}$$

Another way to obtain the mixer conversion gain and the output noise temperature is to calculate it directly from an IF response of HEB mixer to a hot load at an operation point:

$$P_{hot} = k_B\ B\ (T_{295K} + T_{rec})\ \frac{2\ G_m\ G_{LNA}}{L_{opt}} \tag{4.8}$$

where G_{LNA} is a gain of IF chain. A factor "2" appears because of a DSB nature of HEB mixer. If the gain and the noise temperature of IF chain are well known, a mixer conversion gain could be derived from Equation 4.8 as:

$$G_m = \frac{P_{hot}\ L_{opt}}{2\ k_B\ B\ (T_{295K} + T_{rec})\ G_{LNA}} \tag{4.9}$$

And the mixer output noise temperature in this case would be:

$$T_{out} = \frac{P_{hot}\ L_{opt}}{2\ k_B\ B\ G_{LNA}} - T_{LNA} - \frac{2\ G_m\ (T_{295K} + T_{opt})}{L_{opt}} \tag{4.10}$$

4.3 RF measurements at a 1.6 THz LO

4.3.1 Direct response measurements

Before performing noise measurements some preliminary pumping tests of "high" T_c MgB_2 HEB#3 were conducted. The cryostat was placed just in front of the FIR gas laser. The I-V curves of HEB#3 are given in Figure 4.5. The mixer was pumped to the I-V curve close to the optimum with the total available power estimated to be ~100 μW in front of the cryostat (curve 3 in Fig. 4.5(a)). For noise temperature measurements with a thin beam splitter the LO power at the cryostat should be greatly reduced. However, after a better alignment an available LO power was enough to pump a smaller device even with a beam splitter, which is described in the next section. Curves 4 and 2 correspond to the increased bath temperature with and without LO pumping, respectively. For curve 5 LO was switched off and a bath temperature was further increased by the resistive heater until it overlapped with curve 4. The identity of curves 4 and 5 demonstrate that 1.6 THz radiation has the same effect on a HEB as a rise in a bath temperature.

Direct detection experiments were conducted to estimate which I-V curve corresponds to the HEB's maximum sensitivity to the THz radiation. The voltage response of HEB#3 on amplitude modulated THz radiation was recorded for the set of bath temperatures and bias points (see Fig. 4.5(b)).

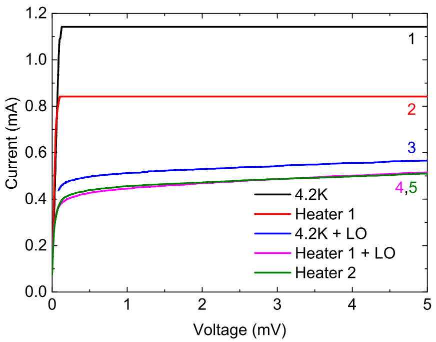

(a)

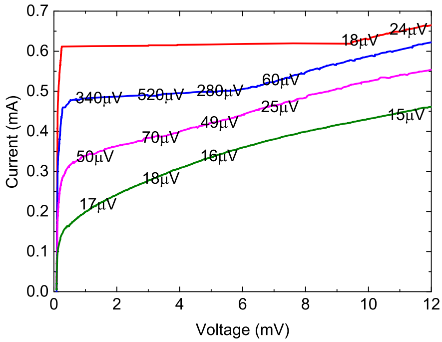

(b)

Fig. 4.5: The I-V curves of HEB#3. (a) Curve 1: 4.2 K without a LO pumping; Curve 2: Heater 1 without a LO pumping; Curve 3: 4.2 K the maximum LO pumping; Curve 4: Heater 1 with the maximum LO pumping; Curve 5: Heater 2, the heating was increased until curve 5 coincided with curve 4. (b) The numbers in the field represent the voltage response on the lock-in amplifier at 1.6THz.

The FIR gas laser radiation was attenuated by 20 dB to reach a small signal limit, when the THz radiation has no visible effect on an I-V curve. The FIR gas laser radiation was also modulated with the chopper set on 20 Hz. The maximum responsivity was achieved at bias points ranging from 2 mV to 4 mV and from 0.3 mA to 0.5 mA, i.e. at 25-35% of the critical current at 4.2 K. Taking into account optical losses the maximum responsivity can be estimated to be in a range of 1–2 kV/W at 1.6 THz.

4.3.2 Mixer noise and gain measurements

HEB#1 was tested using the noise measurement setup described above. The device had a relatively low (for MgB_2) T_c of 8.5 K. Therefore it is of interest for the performance comparison with NbN HEB mixers which have a similar T_c. The I-V curves of HEB#1 at 4.2 K with LO pumping and the corresponding IF response to a 295 K load versus a bias voltage curves are presented in Figures 4.6(a) and 4.6(b).

The required LO power to reach the minimum receiver noise temperature calculated using the isotherm method (LO2 curve in Fig. 4.6(a)) was 70 nW. The isotherm method assumes that both DC and LO powers have the same effect on HEB resistance [77]. The LO power required for the operation in the optimal point is in the same ballpark as one reported for NbN HEB mixers. The DSB receiver noise temperature corrected for optical losses for HEB#1

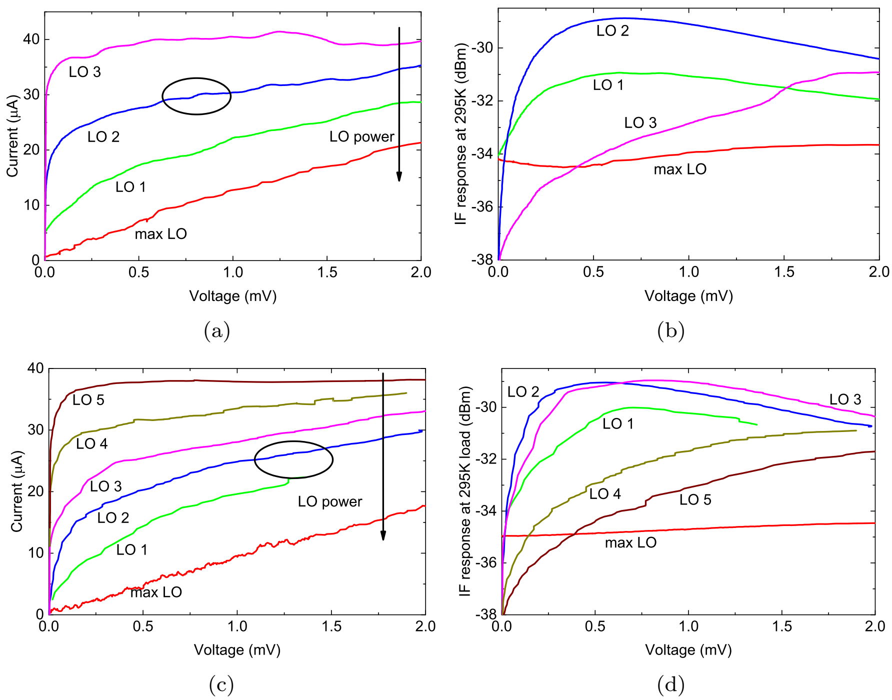

Fig. 4.6: (a) The I-V curves of HEB#1 at 4.2 K under different 1.6 THz LO powers, optimal operation points are marked with a black ellipse and (b) the corresponding IF response to a 295 K load versus a bias voltage at a 1.8 GHz IF. (c) The I-V curves of HEB#1 at 2.7 K under different 1.6 THz LO powers, optimal operation points are marked with a black ellipse and (d) the corresponding IF response to a 295 K load at a 1.8 GHz IF.

versus the IF for the optimal operation point at a 4.2 K bath temperature is presented in Figure 4.7.

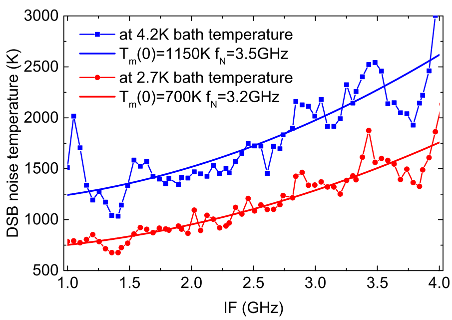

Fig. 4.7: The corrected for optical losses DSB receiver noise temperature of HEB#1 versus the IF at 4.2 K and 2.7 K bath temperatures for a 1.6 THz LO. The bias points are U_0=0.8 mV I_0=28 μA and U_0=1.3 mV I_0=23 μA, respectively.

Table 4.2: THE MIXER CONVERSION GAIN (G_m) AND THE OUTPUT NOISE TEMPERATURE (T_{out}) FOR THE HEB#1 CALCULATED: USING EQ. 4.5 AND 4.7 WITH A SUPERCONDUCTING (I) AND A NORMAL (II) REFERENCE STATE; USING EQ. 4.9 AND 4.10 (III). f_{IF} = 1.8 GHz.

	I		II		III	
T_{bath}(K)	G_m(dB)	T_{out}(K)	G_m(dB)	T_{out}(K)	G_m(dB)	T_{out}(K)
4.2	-19.1	31	-19.6	27	-19.9	26
2.7	-18.2	21	-18.1	22	-18.9	18

HEB#1 was also tested at a bath temperature of 2.7 K. This resulted in a 35% increase of the critical current and a 40% reduction of the receiver noise temperature (see Fig. 4.7). The available LO power was enough to pump the device into a normal state and to perform U-factor measurements. The optimal operation region moved to higher bias voltages. The required LO power was 80 nW. The I-V curves of HEB#1 under LO pumping at 2.7 K and the corresponding IF response curves to a 295 K load are presented in Figures 4.6(c) and 4.6(d).

The corrected DSB noise temperature acquired with Y-factor measurements for HEB#1 was fitted with Equation 2.26. The values of $T_m(0)$ and f_N obtained from a fit are 1150 K and 3.5 GHz for a 4.2 K bath temperature; 700 K and 3.2 GHz for a 2.7 K bath temperature. The measured noise temperature at 2.7 K was much lower then at 4.2 K. However, the reduction of NBW was less significant.

Using the experimental data at 4.2 K from Figure 4.6(b) the mixer conversion gain and the output noise temperature were calculated as it was discussed above. The noise temperature of IF chain was defined mostly by the noise temperature of the first LNA which was mounted on the cryostat's cold plate. The gain of this LNA was 30 dB and the noise temperature was around 2 K. For the whole IF chain the noise temperature was estimated to be not exceeding 3 K. The total gain of IF chain used for the gain method calculation was 77 dB at a 1.8 GHz IF. The IF response at the optimal operation point of U_0=0.8 mV I_0=28 μA (LO2 curve on Fig. 4.6) was -29.4 dBm, which gave U-factor of 8.2 dB for a superconducting state reference and 4.7 dB for a normal state reference. An uncorrected DSB receiver noise temperature of 2500 K and T_{REF}=9 K were taken for a calculation with Equations 4.5 and 4.7.

The results of mixer conversion gain and output noise temperature calculations with all three methods at a 4.2 K bath temperature as well as at a 2.7 K bath temperature are summarized in Table 4.2. Following values were used for the mixer conversion gain and the output noise calculation at a U_0=1.3 mV I_0=23 μA bias point at 2.7 K: an IF response of -30.4 dBm (see Fig. 4.6(d)), U-factor for a superconducting state reference of 7.2 dBm, U-factor for a normal state reference of 4.2 dBm, a receiver noise temperature of 1500 K and T_{REF}=9.3 K.

The values obtained by three methods are very close to each other, which can be interpreted as a confirmation of reliability. While changing the bath temperature from 4.2 K to 2.7 K the mixer conversion gain was increased by

1 dB and the mixer output noise temperature was decreased by 5–10 K. Both of these facts resulted in a decrease of receiver noise temperature. It is interesting to compare this device to a NbN HEB mixer since T_cs are quite close. The reported conversion gain was -12 dB with a mixer output noise temperature of about 40 K [76]. The GBW of HEB#1 is also a factor of 1.5 wider comparing to the NbN HEB [41]. Noise measurements for HEB#1 were performed at a 1.8 GHz IF which is quite close to the 3-dB roll-off frequency. Therefore, a correction of about +2 dB should be applied. Notwithstanding that the receiver noise temperatures are in the same ballpark.

The same experimental setup was used for HEB#2 characterization except a different mixer block and the extra focussing mirror. The thin plastic film was placed between the mixer block and the cryostat's cold plate to minimize a LHe boiling rate during "heated" tests. The I-V curves of HEB#2 at 4.2 K and 12 K with and without a LO pumping are presented in Figure 4.8(a). At a bath temperature of about 12 K the HEB critical current has reduced to the half of its value at 4.2 K. The applied LO power at 12 K was reduced from 2.6 μW to 1.7 μW to get an overlap with the pumped I-V curve at 4.2 K.

The measured receiver noise temperatures across a 1–4 GHz IF band for bath temperatures of 4.2 K and 12 K as well as fits with Equation 2.26 are presented in Figure 4.8(b). Measurements were performed at bias points of U_0=1.6 mV I_0=180 μA and U_0=1.8 mV, I_0=200 μA for 4.2 K and 12 K, respectively. At certain IFs the mixer response on a hot-cold load was unstable, which resulted in errors in noise temperature measurements (e.g. at 3.2 GHz for 12 K and 1.9 GHz, 2.9 GHz for 4.2 K). The corrected receiver noise temperature has increased from 1700 K to 2150 K with an increase of bath temperature but a NBW of 5 GHz left the same.

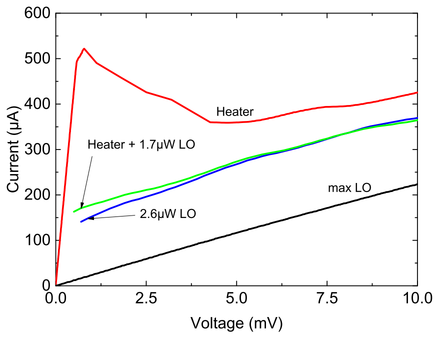

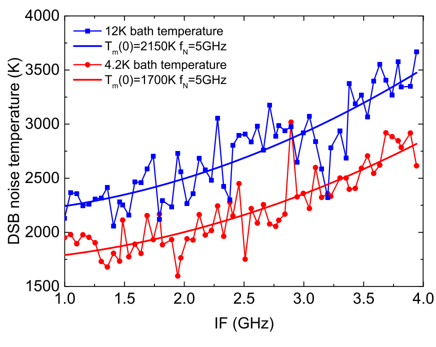

Fig. 4.8: (a) The I-V curves of HEB#2 with and without a 1.6 THz LO power at 12 K and 4.2 K bath temperatures. (b) The corrected for optical losses DSB receiver noise temperatures of HEB#2 versus the IF at 4.2 K(circles) and 12 K (squares) bath temperatures for a 1.6 THz LO. The bias points are U_0=1.6 mV I_0=180 μA and U_0=1.8 mV, I_0=200 μA, respectively.

A direct measurement of GBW at frequencies >1 THz is problematic due to the absence of coherent sources with a tunable frequency. One of the possible solutions is a use of BWOs or multiplier sources with frequencies <1 THz. For

NbN HEB mixers made from ultrathin 3.5 nm films a typical critical temperature is about 9 K. This T_c gives a superconducting gap frequency of about 0.6 THz at 4.2 K. Hence this devices can work with mentioned power sources in regime where a LO frequency is higher than a gap frequency. Consequently this mixing experiments could be extrapolated to higher frequencies.

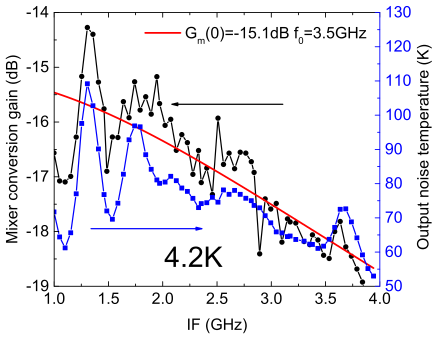

(a)

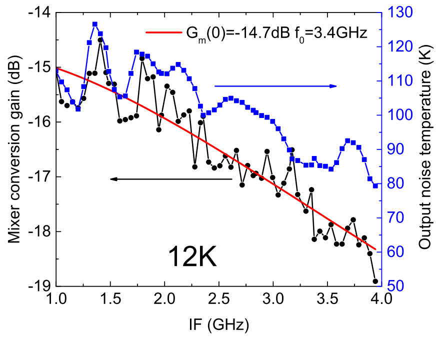

(b)

Fig. 4.9: The measured mixer conversion gain (circles) and output noise temperature (squares) of HEB#2 versus the IF for a 1.6 THz LO at (a) 4.2 K, U_0=1.6 mV I_0=180 μA and (b) 12 K, U_0=1.8 mV, I_0=200 μA.

For a higher T_c results of such low frequency mixing experiments can not be extrapolated to higher frequencies because of slightly different mechanism of mixer operation. In this case low frequency THz radiation is absorbed only in a normal domain of HEB bridge where a superconducting gap is suppresed by a DC power. Instead of mixing experiments for HEB#2 U-factor measurements were performed in a whole IF bandwidth to get a GBW. Moreover, this method provide together with a GBW a mixer conversion gain and an output noise temperature. The results of U-factor measurements for 4.2 K and 12 K bath temperatures are presented in Figure 4.9. Higher ripples for IFs <1.5 GHz correspond to the region of LNA's high return loss. The experimental data of mixer conversion gain were fitted with Equation 2.18. The zero IF mixer conversion gain and the GBW achieved from a fit for 4.2 K and 12 K bath temperatures are -15.1 dB and 3.4 GHz; -14.7 dB and 3.5 GHz, respectively. The HEB shows almost the same conversion gain and GBW at both bath temperatures, but the output noise at a 12 K bath temperature is higher, which resulted in a higher receiver noise temperature. The similar behaviour was observed for HEB#1.

4.4 Preliminary noise measurements at a 2.6 THz LO

Characterisation of MgB_2 HEB with even higher T_c in a mode where a LO frequency is higher then a superconducting gap frequency requires operation at higher bath temperatures or a use of LO sources with higher frequencies. Therefore preliminary Y-factor measurements were performed with HEB#1 at

2.6 THz LO and 2.7 K bath temperature. The available output power from the FIR gas laser at this frequency was lower compared to 1.6 THz but still enough to pump the device. The I-V-curve of HEB#1 pumped with a 2.6 THz LO and the IF response to a 295 K load are plotted in Figure 4.10. Perhaps, this curve does not correspond to the optimal LO pumping, further measurements at this frequency are required.

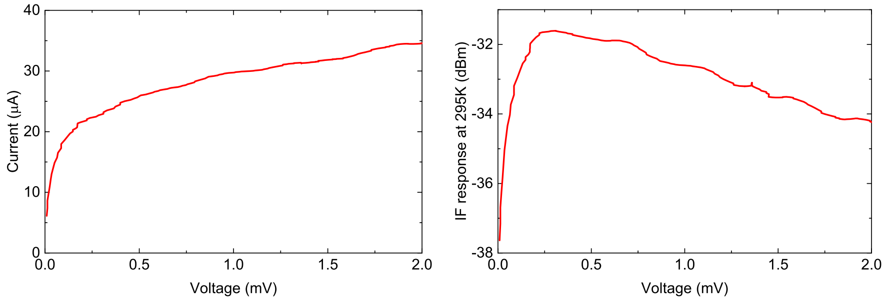

(a) (b)

Fig. 4.10: (a) The I-V curves of HEB#1 under a 2.6 THz LO pumping at 2.7 K and (b) corresponding IF response power to a 295 K load at a 1.8 GHz IF.

The DSB receiver noise temperature versus the IF for a U_0=1.38 mV I_0=31 μA bias point is presented in Figure 4.11. The fit with Equation 2.26 gives a zero IF noise temperature of 1400 K and NBW of 3.7 GHz.

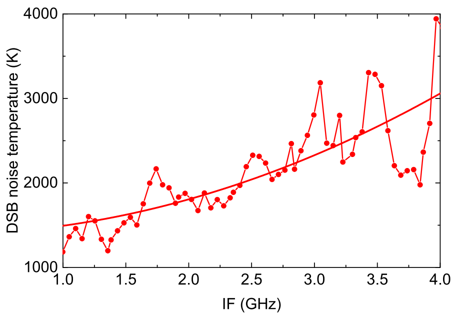

Fig. 4.11: Corrected (for optical losses) DSB receiver noise temperatures versus frequency at 2.7 K bath temperatures for a 2.6 THz LO for HEB#1. The bias point is U_0=1.38 mV and I_0=31 μA.

At a 2.6 THz LO the receiver noise temperature of HEB#1 appears to be higher compared to a 1.6 THz LO, but probably the optimal operation point was not achieved. Further study at this frequency is of great intereset especially for devices with a higher T_c.

4.5 Modelling of MgB_2 HEB mixer gain

The mixer conversion gain for HEB#2 at 4.2 K and 12 K bath temperatures at optimal LO power measured using the gain method for different bias points ("2.6 μW LO" and "1.7 μW LO, heater" I-V curves in Fig. 4.8(a), respectively) are presented in Figure 4.12 (squares). The value of gain is very close to the value achieved with the U-factor measurements for the corresponding bias points.

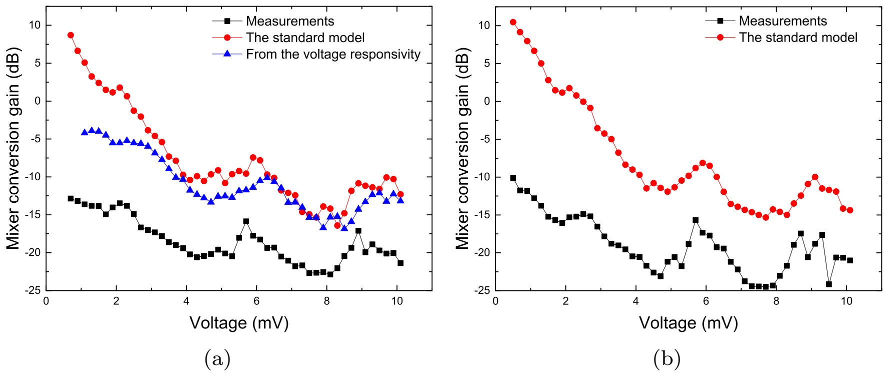

Fig. 4.12: Calculated and modeled mixer conversion gains for HEB#2 at a 1.8 GHz IF at (a) 4.2 K and (b) 12 K bath temperatures.

Using Equation 2.18 the mixer conversion gain for a 1.8 GHz IF and 4.2 K and 12 K bath temperatures was calculated from the I-V curve. The result of calculation is presented in Figure 4.12 (circles). The calculated gain has the same shape as the measured one and similar local maximums at 2 mV, 6 mV and 9 mV. Results are similar to what was presented previously for NbN HEB mixers, where the calculated conversion gain was around 10 dB higher [54] compared to the measured one. It was demonstrated previously that power exchange function χ depends on bias voltage and could be up to 5 for the NbN HEB mixers [54]. Moreover it was demonstrated that χ goes to 1 with increase of voltage because of the growth of normal domain in HEB bridge [52]. Measured and modeled curves differs more at lower bias points, because in these calculations χ was equal to 1.

To get rid of the problem with the overestimated effect of RF radiation on the device the voltage responsivity $R_V(0)$ can be taken from two I-V curves with different LO powers applied. In this case the voltage responsivity would be equal to the bias voltage change along the R_L load line divided by the difference of incident power, which is also calculated with the isotherm method (points b-b') (see Fig. 4.13). The resulted curve is presented in Figure 4.12(a) (blue triangles). The gain calculated in this way is lower than modeled with the standard model at bias points lower than 4 mV. In both cases the assumption that self-heating parameters for the RF and the DC heating are equal was done. In the first case it affects the calculation by the overestimation of RF radiation effect on the HEB and the error in the calculation of P_{LO}. In the second case, the isotherm method is used twice: for the estimation of absorbed power

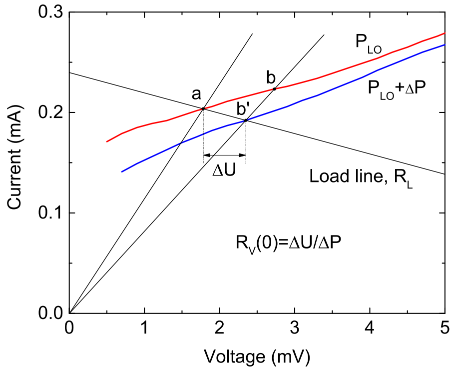

Fig. 4.13: Schematic illustration for the responsivity at zero IF calculation.

difference between two I-V curves and again for the P_{LO} calculation. Moreover, it could be that the assumption that along one I-V curve the absorbed LO power is constant might be wrong. Another thing is that the IF chain gain can change with the bias voltage due to the change of HEB's impedance and the consequent mismatch.

The first attempt to calculate the mixer conversion gain for the MgB_2 was done. Further investigation and more experimental data are required.

Chapter 5

Conclusions and future work

In this thesis, novel HEB mixers for THz frequencies based on MgB_2 has been discussed. **For the thirst time MgB_2 HEBs of the submicron size were fabricated and characterized at frequencies >1 THz.** The switch to submicron sizes allowed for the pumping of MgB_2 HEBs to optimal I-V curves at the LHe temperature using available FIR gas laser. The required LO power for the the device with a "low" T_c of 8.5 K was <100 nW for the LHe bath temperatures. For the HEB with a "high" T_c of 22.5 K the required LO power was measured to be 2.6 μW and 1.7 μW for 4.2 K and 12 K bath temperatures, respectively.

Three different methods: the gain method and U-factor methods with superconducting and normal reference states were applied to estimate the mixer conversion gain an compared. Good agreement with an error margin of $\pm$0.5 dB was demonstrated, which indicates the correctness of methods.

The minimum DSB noise temperature for a "low" T_c HEB was 700 K with a 3.2 GHz NBW and 1150 K with a 3.5 GHz NBW for 2.7 K and 4.2 K bath temperatures respectively. The performance of this device is comparable to NbN HEBs but was achieved with low quality superconducting films. The operation at a bath temperature of 12 K, unachievable with NbN HEB mixers was demonstrated with a 2150 K noise temperature and a 5 GHz NBW. At a bath temperature of 4.2 K the noise temperature reduced to 1700 K keeping a NBW of 5 GHz. The same 3.5 GHz GBW was measured for both bath temperatures. Films with a higher T_c provide a broader NBW as it was discussed previously. The voltage responsivity of such a device was estimated to be 1–2 kV/W at 1.6 THz. The experimental results indicated that MgB_2 HEB mixers with a T_c >30–35 K could push the operation temperature above 20 K with no or acceptable sensitivity reduction.

Fabricated devices with a SiN_x passivation demonstrated high robustness and did not lose their properties after continuous storage in a nitrogen atmosphere. However, for a space applications special reliability tests are required.

It is absolutely clear that a further development of MgB_2 HEB mixers is necessary. A good sensitivity and a large bandwidth have been already demonstrated on different devices separately. The combination of both of these parameters in one device would provide the perfect instrument for the sub-mm wave astronomy. Further steps in MgB_2 HEB mixers development are:

- Testing of devices from the already fabricated batches N2, N4 and N5. This will provide more experimental data to study MgB_2 HEB mixers behaviour.
- Application of the HEB mixer model to a larger amount of experimental data. Use of hot-spot models is required for the correct noise calculation.
- Performing of noise measurements at higher LO frequencies up to 5 THz which are wittingly higher than the superconducting gap frequency of MgB_2.
- Development and optimisation of MgB_2 thin film deposition on a recently launched HPCVD system at Chalmers University of Technology. HPCVD thin film deposition with a consequent ion beam milling seems to be very promising for ultra-thin film fabrication for superconducting devices.

Chapter 6

Summary of appended papers

Paper A

MgB_2 hot-electron bolometer mixers at terahertz frequencies

The results of direct responsivity characterisation of MgB_2 HEB mixer with a critical temperature of 20 K made from 20 nm film are presented. I personally contributed with: design and processing of HEB, measurements, analysis of the data. The responsivity measurements were performed with help of my supervisor Sergey Cherednichenko and Stella Bevilacqua.

Paper B

Noise measurements of the low T_c MgB_2 HEB mixer at 1.6 THz and 2.6 THz

In this paper, noise temperatures of 700 K and 1150 K measured at 2.7 K and 4.2 K, respectively, at a 1.6 THz local oscillator and 1400 K at 2.7 K at a 2.6 THz local oscillator using HEB mixer made with a critical temperature of 8.5 K from 10 nm MgB_2 film are reported. I personally contributed with: measurements, analysis of the data and writing. The RF measurements were performed with help of my supervisor Sergey Cherednichenko and Stella Bevilacqua.

Paper C

Effect of the critical and operational temperatures on the sensitivity of MgB_2 HEB mixers

In this paper, results of the noise and gain bandwidth investigation of HEB mixer made from 20 nm MgB_2 film with a critical temperature of 22.5 K are presented. I personally contribute with: design and processing of HEB, measurements, analysis of the data and writing. The RF measurements were performed with help of my supervisor Sergey Cherednichenko and Stella Bevilacqua.

Acknowledgment

This work would never be dome without people I have worked with during my PhD study.

First and foremost, I would like to express my deep gratitude to my supervisor Assoc. Prof. Sergey Cherednichenko for guidance, discussions and help with measurements and data analysis, which made this work possible. My sincere thanks to my examiner Professor Jan Stake for his support and for giving me the possibility to do the PhD at the Terahertz and Millimetre Wave Laboratory. Many special thanks to my colleague Stella Bevilacqua for the fruitful discussions, for guidance and help in the process lab and for assisting me in the measurement lab. In addition, I want to thank Vladimir Drakinskiy for helpful discussions, teaching me in the process lab and giving me lots of hints about the processing.

Hiroyuki Shibata and Professor Yasuhiro Tokura from NTT Basic Research Laboratories, are acknowledged for the material providing.

I want to thank all the staff of the Nanofabrication Laboratory. In particular, Henrik Frederiksen for the great help with the construction of the HPCVD deposition system.

Special thanks to my parents for the encouraging and support.

This work was financially supported by the European Research Council (ERC) under a Consolidator type grant TERAMIX.

Bibliography

[1] A. Rogalski and F. Sizov, "Terahertz detectors and focal plane arrays," *Opto-Electronics Review*, vol. 19, no. 3, pp. 346–404, Sep 2011.

[2] R. A. Lewis, "A review of terahertz sources," *Journal of Physics D: Applied Physics*, vol. 47, no. 37, p. 374001, Sep 2014.

[3] P. Siegel, "Terahertz technology in biology and medicine," *IEEE Transactions on Microwave Theory and Techniques*, vol. 52, no. 10, pp. 2438–2447, Oct 2004.

[4] M. C. Kemp, P. F. Taday, B. E. Cole, J. A. Cluff, A. J. Fitzgerald, and W. R. Tribe, "Security applications of terahertz technology," *Proc. SPIE*, vol. 5070, pp. 44–52, 2003.

[5] M. Fitch and R. Osiander, "Terahertz waves for communications and sensing," *Johns Hopkins APL Technical Digest (Applied Physics Laboratory)*, vol. 25, no. 4, pp. 348–355, 2004.

[6] T. Phillips and J. Keene, "Submillimeter astronomy," *Proceedings of the IEEE*, vol. 80, no. 11, pp. 1662–1678, Nov 1992.

[7] G. Stacey, "THz Low Resolution Spectroscopy for Astronomy," *IEEE Transactions on Terahertz Science and Technology*, vol. 1, no. 1, pp. 241–255, Sept 2011.

[8] P. Ubertini, N. Gehrels, I. Corbett, P. de Bernardis, M. Machado, M. Griffin, M. Hauser, R. K. Manchanda, N. Kawai, S.-N. Zhang, and M. Pavlinsky, "Future of Space Astronomy: A global Road Map for the next decades," *Advances in space research*, vol. 50, no. 1, pp. 1–55, Jul 2012.

[9] H.-W. Hübers, "Terahertz Heterodyne Receivers," *IEEE Journal of Selected Topics in Quantum Electronics*, vol. 14, no. 2, pp. 378–391, Mar-Apr 2008.

[10] J. Zmuidzinas and P. Richards, "Superconducting detectors and mixers for millimeter and submillimeter astrophysics," *Proceedings of the IEEE*, vol. 92, no. 10, pp. 1597–1616, Oct 2004.

[11] E. Gershenzon, G. Gol´tsman, I. Gogidze, Y. Gusev, A. Elantev, B. Karasik, and A. Semenov, "Millimeter and submillimeter range mixer based on electronic heating of superconductive films in the resistive state," *Superconductivity*, vol. 10, no. 3, pp. 1582–1597, Oct 1990.

[12] E. Gershenzon, M. Gershenzon, G. Gol'tsman, A. Semyonov, and A. Sergeev, "Heating of electrons in superconductor in the resistive state due to electromagnetic radiation," *Solid State Communications*, vol. 50, no. 3, pp. "207–212, 1984.

[13] K. Zhou, W. Miao, Z. Lou, J. Hu, S. Li, W. Zhang, S. Shi, R. Lefevre, Y. Delorme, and T. Vacelet, "A 1.4 THz Quasi-Optical NbN Superconducting HEB Mixer Developed for the DATE5 Telescope," *IEEE Transactions on Applied Superconductivity*, vol. 25, no. 3, pp. 1–5, Jun 2015.

[14] W. Zhang, P. Khosropanah, J. R. Gao, T. Bansal, T. M. Klapwijk, W. Miao, and S. C. Shi, "Noise temperature and beam pattern of an NbN hot electron bolometer mixer at 5.25 THz," *Journal of Applied Physics*, vol. 108, no. 9, p. 093102, Nov 2010.

[15] D. Marrone, R. Blundell, E. Tong, S. Paine, D. Loudkov, J. Kawamura, D. Lühr, and C. Barrientos, "Observations in the 1.3 and 1.5 THz Atmospheric Windows with the Receiver Lab Telescope," in *16th International Symposium on Space Terahertz Technology*, May 2005, pp. 64–67.

[16] D. Meledin, A. Pavolotsky, V. Desmaris, I. Lapkin, C. Risacher, V. Perez, D. Henke, O. Nystrom, E. Sundin, D. Dochev, M. Pantaleev, M. Fredrixon, M. Strandberg, B. Voronov, G. Goltsman, and V. Belitsky, "A 1.3-THz Balanced Waveguide HEB Mixer for the APEX Telescope," *IEEE Transactions on Microwave Theory and Techniques*, vol. 57, no. 1, pp. 89–98, Jan 2009.

[17] C. Risacher, D. Meledin, V. Belitsky, and P. Bergman, "First 1.3 THz Observations at the APEX Telescope," in *20th International Symposium on Space Terahertz Technology*, Apr 2009, pp. 54–61.

[18] T. de Graauw et al., "The Herschel-Heterodyne Instrument for the Far-Infrared (HIFI)," *Astronomy & Astrophysics*, vol. 518, p. L6, Jul-Aug 2010.

[19] P. Goldsmith and D. Lis, "Early Science Results From the Heterodyne Instrument for the Far Infrared (HIFI) on the Herschel Space Observatory," *Terahertz Science and Technology, IEEE Transactions on*, vol. 2, no. 4, pp. 383–392, Jul 2012.

[20] M. Suttiwong, M. Birk, G. Wagner, M. Krocka, M. Wittkamp, P. Haschberger, P. Vogt, and F. Geiger, "Development and Characterization of the Balloon Borne Instrument Telis (Terahertz and Submm Limb Sounder): 1.8 THz Receiver," in *19th ESA Symposium on European Rocket and Balloon Programmes and Related Research*, Jun 2009.

[21] M. Birk, G. Wagner, G. de Lange, A. de Lange, B. N. Ellison, M. Harman, A. Murk, H. Oelhaf, G. Maucher, and C. Sartorius, "TELIS: TErahertz and subMMW LImb Sounder — Project Summary After First Successful Flight," in *21th International Symposium on Space Terahertz Technology*, Mar 2010, pp. 195–200.

[22] S. Heyminck, U. U. Graf, R. Güsten, J. Stutzki, H. W. Hübers, and P. Hartogh, "GREAT: the SOFIA high-frequency heterodyne instrument," *Astronomy & Astrophysics*, vol. 542, p. L1, Jun 2012.

[23] D. Buchel, P. Putz, K. Jacobs, M. Schultz, U. Graf, C. Risacher, H. Richter, O. Ricken, H.-W. Hubers, R. Gusten, C. Honingh, and J. Stutzki, "4.7-THz Superconducting Hot Electron Bolometer Waveguide Mixer," *Terahertz Science and Technology, IEEE Transactions on*, vol. 5, no. 2, pp. 207–214, Mar 2015.

[24] L. Jiang, S. Shiba, T. Shiino, K. Shimbo, N. Sakai, T. Yamakura, Y. Irimajiri, P. G. Ananthasubramanian, H. Maezawa, and S. Yamamoto, "Development of 1.5 THz waveguide NbTiN superconducting hot electron bolometer mixers," *Superconductor Science and Technology*, vol. 23, no. 4, p. 045025, Apr 2010.

[25] A. F. Loenen et al., "Excitation of the molecular gas in the nuclear region of M82," *Astronomy & Astrophysics*, vol. 521, p. L2, Oct 2010.

[26] J. Nagamatsu, N. Nakagawa, T. Muranaka, Y. Zenitani, and J. Akimitsu, "Superconductivity at 39 K in magnesium diboride," *Nature*, vol. 410, no. 6824, pp. 63–64, Mar 2001.

[27] W. N. Kang, H.-J. Kim, E.-M. Choi, C. U. Jung, and S.-I. Lee, "MgB_2 Superconducting Thin Films with a Transition Temperature of 39 Kelvin," *Science*, vol. 292, no. 5521, pp. 1521–1523, May 2001.

[28] X. Zeng, A. Pogrebnyakov, A. Kotcharov, J. Jones, X. Xi, E. Lysczek, J. Redwing, X. Shengyong, Q. Li, J. Lettieri, D. Schlom, W. Tian, X. Pan, and Z.-K. Liu, "In situ epitaxial MgB_2 thin films for superconducting electronics," *Nature Materials*, vol. 1, no. 1, pp. 35–38, Sep 2002.

[29] K. Ueda and M. Naito, "In situ growth of superconducting MgB_2 thin films by molecular-beam epitaxy," *Journal of Applied Physics*, vol. 93, no. 4, pp. 2113–2120, Feb 2003.

[30] S. Cherednichenko, V. Drakinskiy, K. Ueda, and M. Naito, "Terahertz mixing in MgB_2 microbolometers," *Applied Physics Letters*, vol. 90, no. 2, Jan 2007.

[31] S. Bevilacqua, S. Cherednichenko, V. Drakinskiy, H. Shibata, A. Hammar, and J. Stake, "Investigation of MgB_2 HEB mixer gain bandwidth," in *IRMMW-THz 2011 - 36th International Conference on Infrared, Millimeter, and Terahertz Waves*, Oct 2011, pp. 1–2.

[32] S. Bevilacqua, S. Cherednichenko, V. Drakinskiy, J. Stake, H. Shibata, and Y. Tokura, "Low noise mgb_2 terahertz hot-electron bolometer mixers," *Applied Physics Letters*, vol. 100, no. 3, p. 033504, Jan 2012.

[33] S. Bevilacqua, S. Cherednichenko, V. Drakinskiy, H. Shibata, Y. Tokura, and J. Stake, "Study of if bandwidth of mgb_2 phonon-cooled hot-electron bolometer mixers," *IEEE Transactions on Terahertz Science and Technology*, vol. 3, no. 4, pp. 409–415, Jul 2013.

[34] H. Shibata, T. Maruyama, T. Akazaki, H. Takesue, T. Honjo, and Y. Tokura, “Photon detection and fabrication of MgB_2 nanowire,” *Physica C: Superconductivity*, vol. 468, no. 15-20, pp. 1992–1994, Sep 2008.

[35] D. Cunnane, J. Kawamura, M. Wolak, N. Acharya, T. Tan, X. Xi, and B. Karasik, “Characterization of mgb_2 superconducting hot electron bolometers,” *Applied Superconductivity, IEEE Transactions on*, vol. 25, no. 3, p. 2300206, Jun 2015.

[36] X. Xi, A. Pogrebnyakov, S. Xu, K. Chen, Y. Cui, E. Maertz, C. Zhuang, Q. Li, D. Lamborn, J. Redwing, Z. Liu, A. Soukiassian, D. Schlom, X. Weng, E. Dickey, Y. Chen, W. Tian, X. Pan, S. Cybart, and R. Dynes, “MgB_2 thin films by hybrid physical-chemical vapor deposition,” *Physica C: Superconductivity*, vol. 456, no. 1-2, pp. 22–37, Jun 2007.

[37] P. L. Richards, “Bolometers for infrared and millimeter waves,” *Journal of Applied Physics*, vol. 76, no. 1, Jul 1994.

[38] F. Arams, C. Allen, B. Peyton, and E. Sard, “Millimeter mixing and detection in bulk InSb,” *Proceedings of the IEEE*, vol. 54, no. 4, pp. 612–622, Apr 1966.

[39] T. G. Phillips and K. B. Jefferts, “A Low Temperature Bolometer Heterodyne Receiver for Millimeter Wave Astronomy,” *Review of Scientific Instruments*, vol. 44, no. 8, pp. 1009–1014, Aug 1973.

[40] Y. P. Gousev, G. N. Gol’tsman, A. D. Semenov, E. M. Gershenzon, R. S. Nebosis, M. A. Heusinger, and K. F. Renk, “Broadband ultrafast superconducting NbN detector for electromagnetic radiation,” *Journal of Applied Physics*, vol. 75, no. 7, Apr 1994.

[41] S. Cherednichenko, P. Khosropanah, E. Kollberg, M. Kroug, and H. Merkel, “Terahertz superconducting hot-electron bolometer mixers,” *Physica C: Superconductivity*, vol. 372-376, no. 1, pp. 407–415, Aug 2002.

[42] D. E. Prober, “Superconducting terahertz mixer using a transition-edge microbolometer,” *Applied Physics Letters*, vol. 62, no. 17, pp. 2119–2121, Apr 1993.

[43] A. Semenov, G. Gol’tsman, and R. Sobolewski, “Hot-electron effect in superconductors and its applications for radiation sensors,” *Superconductor Science and Technology*, vol. 15, no. 4, pp. R1–R16, Mar 2002.

[44] N. Perrin and C. Vanneste, “Response of superconducting films to a periodic optical irradiation,” *Phys. Rev. B*, vol. 28, pp. 5150–5159, Nov 1983.

[45] B. S. Karasik and A. I. Elantiev, “Noise temperature limit of a superconducting hot electron bolometer mixer,” *Applied Physics Letters*, vol. 68, no. 6, pp. 853–855, Feb 1996.

[46] H. Merkel, P. Khosropanah, P. Yagoubov, and E. Kollberg, “A hot-spot mixer model for phonon-cooled NbN hot electron bolometric mixers,” *Applied Superconductivity, IEEE Transactions on*, vol. 9, no. 2, pp. 4201–4204, June 1999.

[47] H. Merkel, P. Khosropanah, D. Wilms Floet, P. Yagoubov, and E. Kollberg, "Conversion gain and fluctuation noise of phonon-cooled hot-electron bolometers in hot-spot regime," *Microwave Theory and Techniques, IEEE Transactions on*, vol. 48, no. 4, pp. 690–699, Apr 2000.

[48] H. Merkel, P. Khosropanah, S. Cherednichenko, K. Yngvesson, A. Adam, and E. Kollberg, "A two-dimensional hot-spot mixer model for phonon-cooled hot electron bolometers," *Applied Superconductivity, IEEE Transactions on*, vol. 11, no. 1, pp. 179–182, Mar 2001.

[49] B. S. Karasik and A. Elantev, "Analysis of the Noise Performance of a Hot-Electron Superconducting Bolometer Mixer," in *6th International Symposium on Space Terahertz Technology*, Mar 1995, pp. 229–246.

[50] H. Ekström, B. Karasik, E. Kollberg, and K. Yngvesson, "Conversion gain and noise of niobium superconducting hot-electron-mixers," *IEEE Transactions on Microwave Theory and Techniques*, vol. 43, no. 4, pp. 938–947, Apr 1995.

[51] S. Bevilacqua, E. Novoselov, S. Cherednichenko, H. Shibata, and Y. Tokura, "Wideband MgB_2 Hot-Electron Bolometer Mixers: IF Impedance Characterisation and Modeling," *Submitted to IEEE Transactions on Applied Superconductivity*, 2015.

[52] J. W. Kooi, J. J. A. Baselmans, M. Hajenius, J. R. Gao, T. M. Klapwijk, P. Dieleman, A. Baryshev, and G. de Lange, "IF impedance and mixer gain of NbN hot electron bolometers," *Journal of Applied Physics*, vol. 101, no. 4, p. 044511, Feb 2007.

[53] H. Merkel, P. Yagoubov, P. Khosropanah, and E. Kollberg, "An accurate calculation method of the absorbed LO power in hot electron bolometric mixers," in *Terahertz Electronics Proceedings, 1998. THz Ninety Eight. 1998 IEEE Sixth International Conference on*, Sep 1998, pp. 145–148.

[54] P. Khosropanah, H. Merkel, S. Yngvesson, A. Adam, S. Cherednichenko, and E. Kollberg, "A distributed device model for phonon-cooled HEB mixers predicting IV characteristics, gain, noise and IF bandwidth," in *11th International Symposium on Space Terahertz Technology*, May 2000, pp. 474–488.

[55] J. C. Mather, "Bolometer noise: nonequilibrium theory," *Appl. Opt.*, vol. 21, no. 6, pp. 1125–1129, Mar 1982.

[56] H. Shibata, T. Akazaki, and Y. Tokura, "Fabrication of MgB_2 Nanowire Single-Photon Detector with Meander Structure," *Applied Physics Express*, vol. 6, no. 2, p. 023101, Feb 2013.

[57] D. Cunnane, E. Galan, K. Chen, and X. X. Xi, "Planar-type MgB_2 SQUIDs utilizing a multilayer process," *Applied Physics Letters*, vol. 103, no. 21, p. 212603, Nov 2013.

[58] Y. Xu, M. Khafizov, L. Satrapinsky, P. Kus, A. Plecenik, and R. Sobolewski, "Time-resolved photoexcitation of the superconducting

two-gap state in MgB_2 thin films," *Physical Review Letters*, vol. 91, no. 19, p. 197004, Nov 2003.

[59] Y. Naidyuk, I. Yanson, L. Tyutrina, N. Bobrov, P. Chubov, W. Kang, H.-J. Kim, E.-M. Choi, and S.-I. Lee, "Superconducting energy gap distribution in c-axis oriented MgB_2 thin film from point contact study," *Journal of Experimental and Theoretical Physics Letters*, vol. 75, no. 5, pp. 238–241, Mar 2002.

[60] S. D. Bu, D. M. Kim, J. H. Choi, J. Giencke, E. E. Hellstrom, D. C. Larbalestier, S. Patnaik, L. Cooley, C. B. Eom, J. Lettieri, D. G. Schlom, W. Tian, and X. Q. Pan, "Synthesis and properties of c-axis oriented epitaxial MgB_2 thin films," *Applied Physics Letters*, vol. 81, no. 10, pp. 1851–1853, Nov 2002.

[61] Y. Zhang, Z. Lin, Q. Dai, D. Li, Y. Wang, Y. Zhang, Y. Wang, and Q. Feng, "Ultrathin MgB_2 films fabricated on Al_2O_3 substrate by hybrid physical-chemical vapor deposition with high T_c and J_c," *Superconductor Science and Technology*, vol. 24, no. 1, p. 015013, 2011.

[62] M. A. Wolak, N. Acharya, D. P. Cunnane, B. S. Karasik, and X. X. Xi, "Ultrathin MgB_2 Films for Hot Electron Bolometer Mixers Fabricated by HPCVD and Ion Milling," in *26th International Symposium on Space Terahertz Technology*, Mar 2015, pp. P–43.

[63] D. Cunnane, J. Kawamura, B. Karasik, M. Wolak, and X. Xi, "Development of hot-electron THz bolometric mixers using MgB_2 thin films," vol. 9153, 2014.

[64] Y. Cui, J. Jones, A. Beckley, R. Donovan, D. Lishego, E. Maertz, A. Pogrebnyakov, P. Orgiani, J. Redwing, and X. Xi, "Degradation of MgB_2 thin films in water," *IEEE Transactions on Applied Superconductivity*, vol. 15, no. 2, pp. 224–227, Jun 2005.

[65] R. K. Singh, Y. Shen, R. Gandikota, J. M. Rowell, and N. Newman, "Effect of stoichiometry on oxygen incorporation in MgB_2 thin films," *Superconductor Science and Technology*, vol. 21, no. 1, p. 015018, Jan 2008.

[66] H. Shibata, T. Akazaki, and Y. Tokura, "Ultrathin MgB_2 films fabricated by molecular beam epitaxy and rapid annealing," *Superconductor Science and Technology*, vol. 26, no. 3, p. 035005, Mar 2013.

[67] J. Zmuidzinas and H. LeDuc, "Quasi-optical slot antenna SIS mixers," *Microwave Theory and Techniques, IEEE Transactions on*, vol. 40, no. 9, pp. 1797–1804, Sep 1992.

[68] S. Masarweh, T. Sherer, K. Yngvesson, R. Gingras, C. Drubin, A. G. Cardiasmenos, and J. Wolverton, "Modeling of a monolithic slot ring quasi-optical mixer," *Microwave Theory and Techniques, IEEE Transactions on*, vol. 42, no. 9, pp. 1602–1609, Sep 1994.

[69] S. Gearhart, J. Hesler, W. Bishop, T. Crowe, and G. Rebeiz, "A wide-band 760-GHz planar integrated Schottky receiver," *Microwave and Guided Wave Letters, IEEE*, vol. 3, no. 7, pp. 205–207, Jul 1993.

[70] T. Buttgenbach, "An improved solution for integrated array optics in quasi-optical mm and submm receivers: the hybrid antenna," *Microwave Theory and Techniques, IEEE Transactions on*, vol. 41, no. 10, pp. 1750–1760, Oct 1993.

[71] G. Reppel and E. Saur, "Superconducting proximity effect of NbN," *Journal of Low Temperature Physics*, vol. 17, no. 3-4, pp. 287–293, Nov 1974.

[72] M. Wolak, N. Acharya, T. Tan, D. Cunnane, B. Karasik, and X. Xi, "Fabrication and Characterization of Ultrathin MgB_2 Films for Hot-Electron Bolometer Applications," *Applied Superconductivity, IEEE Transactions on*, vol. 25, no. 3, pp. 1–5, Jun 2015.

[73] I. Mazin, O. Andersen, O. Jepsen, O. Dolgov, J. Kortus, A. Golubov, A. Kuz'menko, and D. M. van der, "Superconductivity in MgB_2: Clean or Dirty?" *Physical Review Letters*, vol. 89, no. 10, p. 107002, Sep 2002.

[74] M. Putti, V. Braccini, E. Galleani, F. Napoli, I. Pallecchi, A. S. Siri, P. Manfrinetti, and A. Palenzona, "Two-band effects in the transport properties of MgB_2," *Superconductor Science and Technology*, vol. 16, no. 2, pp. 188–192, Feb 2003.

[75] J. H. Jung, K. W. Kim, H. J. Lee, M. W. Kim, T. W. Noh, W. N. Kang, H.-J. Kim, E.-M. Choi, C. U. Jung, and S.-I. Lee, "Far-infrared transmission studies of a c-axis-oriented superconducting MgB_2 thin film," *Phys. Rev. B*, vol. 65, p. 052413, Jan 2002.

[76] S. Cherednichenko, M. Kroug, H. Merkel, P. Khosropanah, A. Adam, E. Kollberg, D. Loudkov, G. Gol'tsman, B. Voronov, H. Richter, and H.-W. Huebers, "1.6 THz heterodyne receiver for the far infrared space telescope," *Physica C: Superconductivity*, vol. 372-376, no. 1, pp. 427–431, Aug 2002.

[77] G. Gol'tsman, B. Karasik, O. Okunev, A. Dzardanov, E. Gershenzon, H. Ekstrom, S. Jacobsson, and E. Kollberg, "NbN hot electron superconducting mixers for 100 GHz operation," *IEEE Transactions on Applied Superconductivity*, vol. 5, no. 2, pp. 3065–3068, June 1995.